Chapter 22

Ultrafast Force-Clamp Spectroscopy of Microtubule-Binding Proteins

Suvranta K. Tripathy, Vladimir M. Demidov, Ivan V. Gonchar, Shaowen Wu, Fazly I. Ataullakhanov, and Ekaterina L. Grishchuk

Abstract

Optical trapping has been instrumental for deciphering translocation mechanisms of the force-generating cytoskeletal proteins. However, studies of the dynamic interactions between microtubules (MTs) and MT-associated proteins (MAPs) with no motor activity are lagging. Investigating the motility of MAPs that can diffuse along MT walls is a particular challenge for optical-trapping assays because thermally driven motions rely on weak and highly transient interactions. Three-bead, ultrafast force-clamp (UFFC) spectroscopy has the potential to resolve static and diffusive translocations of different MAPs with sub-millisecond temporal resolution and sub-nanometer spatial precision. In this report, we present detailed procedures for implementing UFFC, including setup of the optical instrument and feedback control, immobilization and functionalization of pedestal beads, and preparation of MT dumbbells. Example results for strong static interactions were generated using the Kinesin-7 motor CENP-E in the presence of AMP-PNP. Time resolution for MAP–MT interactions in the UFFC assay is limited by the MT dumbbell relaxation time, which is significantly longer than reported for analogous experiments using actin filaments. UFFC, however, provides a unique opportunity for quantitative studies on MAPs that glide along MTs under a dragging force, as illustrated using the kinetochore-associated Ska complex.

Key words Bead functionalization, CENP-E kinesin, Kinetochore, Microtubule-associated proteins, Microtubule-dependent diffusion, Molecular friction, Ska complex, Ultrafast force-clamp spectroscopy

Abbreviations

AOD	Acousto-optic deflector
BG	Biotinylated benzylguanine
b-PEG	Biotin polyethylene glycol
BSA	Bovine serum albumin

Suvranta K. Tripathy and Vladimir M. Demidov have equal first-author contribution.

Fazly I. Ataullakhanov and Ekaterina L. Grishchuk contributed equally to developing and implementing this work.

Arne Gennerich (ed.), *Optical Tweezers: Methods and Protocols*, Methods in Molecular Biology, vol. 2478,
https://doi.org/10.1007/978-1-0716-2229-2_22,

DTT	Dithiothreitol
FPGA	Field-programmable gate array
GBP	GFP-binding protein
MAP	Microtubule-associated protein
MT	Microtubule
QPD	Quadrant photo-detector
SD	Standard deviation
UFFC	Ultrafast force-clamp

1 Introduction

Microtubule-associated proteins (MAPs) contribute to a wide range of cellular functions, such as regulating the stability and dynamic behaviors of the microtubule (MT) cytoskeleton [1–3], motor-dependent transport of cellular organelles [4, 5], and the structure and function of neurons [6–8]. During cell division, MAPs play essential roles in regulating spindle formation and dynamics. They also transmit forces from depolymerizing MTs to chromosomes to drive their poleward motions [9, 10]. Spindle MTs attach to kinetochores, macromolecular structures that couple chromosomes to growing or shrinking MT ends [11, 12]. As MTs translocate through their attachment sites at the kinetochores, transient bonds between the kinetochore-associated MAPs and polymerized tubulins permit continuous kinetochore gliding along MTs while generating molecular friction [13–15].

The frictional force arises from breaking of the bonds between MTs and a MAP as it glides, a process akin to facilitated diffusion [15–17]. Several MAPs, including kinesin-8 in the presence of ADP, have been shown to form diffusive bonds on the MT wall and exert frictional resistance to the drag force along the MT in vitro [17–22]. The exact mechanisms that underlie the diffusion and force-dependent gliding of a MAP on the MT wall are not fully understood. Such translocations are likely to involve electrostatic interactions between negatively charged tubulin tails and positively charged unstructured extensions and amino acid patches, which are common in MAPs [23, 24]. Kinesin-8, however, appears to translocate under the dragging force via a hand-over-hand mechanism. Its 8-nm force-induced "step" in the presence of ADP [17] is in contrast to the 4-nm step size expected from tubulin-tail-dependent translocation, indicating that Kinesin-8 uses a different gliding mechanism. Because most diffusing MAPs are not homodimers like kinesin-8, and their MT-dependent diffusion coefficients vary considerably [17, 25–27], different mechanisms of MAP translocation are likely to exist. Understanding how MAPs glide on MTs under dragging force is crucial for understanding fundamental mechanisms of chromosome motility, as well as other MT-dependent cellular functions.

Recent advances in the spatial and temporal resolutions of optical-tweezers systems have led to various measurement strategies, from single trapped bead to three-bead assays in static or dynamic configurations [28–44] (Fig. 1). These versatile assays have been successfully applied to dissect the interactions between molecular motors and their respective filaments, enabling determination of critical characteristics such as force-velocity and force-dependent detachment rate [33–37]. Some of these methodologies have also been applied to study MAP molecules with no motor activity. Static MAP–MT interactions can be interrogated using a single-trap geometry, enabling determination of the release rate and unbinding force of high-affinity interactions [38–41], although identifying the exact binding time and MAP position using this assay may be challenging. A single-trap assay has also been applied to study diffusive MAPs (Fig. 1a). In this case, the coverslip-immobilized MT filament is mechanically dragged by moving the stage at a constant velocity, thereby creating frictional force on the bead-bound MAP [17, 19]. This approach has provided a great deal of information about the abilities of different MAPs to glide under force. However, several factors limit the applicability of this trapping technique. One known issue is that the MAP-coated microbeads can roll on the surface of the MT [18]. Rotational motion is expected during the initial movement of a microsphere in the trap, which applies force to the center of the bead, whereas the MT-bound MAP molecule is located on the bead's surface [45–47]. This initial torque encourages the bead to roll and exerts a tangential force on the MT-bound molecule, potentially decreasing its MT-binding time. Because multiple molecules are found on the bead surface, the recorded bead motion may represent a complex mix of multimolecular rotational motility and single-molecule gliding. Such a scenario can be ruled out for strongly binding MAPs with low diffusion coefficients by directly observing translocation steps, as for kinesin-8 [17], but most MAPs diffuse much faster and resolving their stepping is difficult.

The issue described above is mitigated using the three-bead assay, in which a dumbbell is formed by connecting a filament such as an MT or actin filament between two optically trapped beads (Fig. 1b). Proteins of interest are coated onto to a third bead (pedestal) immobilized on the coverslip. The stage is oscillated to apply force when the filament interacts with the molecules on the pedestal, which cannot roll along the MT [42, 43, 48]. Another advantage of this geometry is that the force is applied parallel to the filament [49], which is physiologically relevant to the interaction geometry of kinetochore-bound MAPs on spindle MTs during chromosome motion. Although such a three-bead approach has not yet been used to study MAPs, it was highly successful for dissecting force-sensitivity of actin-binding proteins involved in cell adhesion [42, 43].

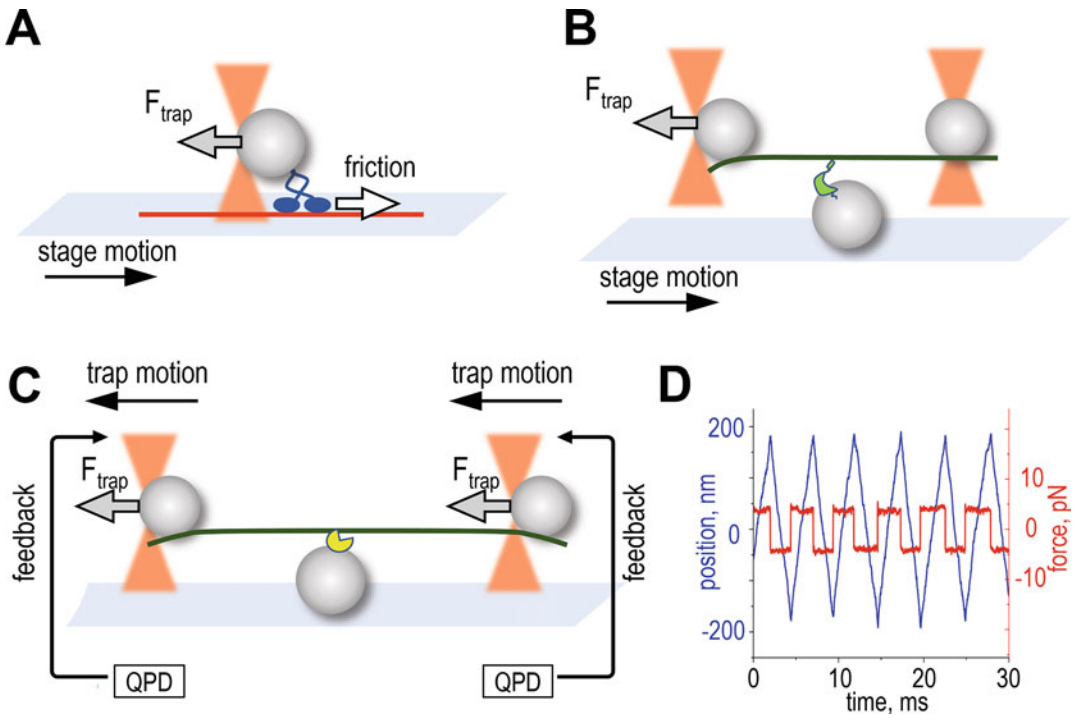

Fig. 1 Optical-trapping configurations to study force-dependent interactions between filaments and proteins with no motor activity. (**a**) A stationary trap holds a MAP-coated bead, which slides on a coverslip-immobilized MT, generating molecular friction [17, 19]. (**b**) Three-bead assay employing actin dumbbell and pedestal coated with high-affinity actin-binding molecules [42, 43]. (**c**) UFFC assay uses the three-bead geometry in combination with a feedback regime for ultrafast force application to actin-binding and DNA-binding proteins [44]. (**d**) Example UFFC recording for control MT dumbbell at 4 pN force clamp. Position of one of the dumbbell beads is shown in blue. Trapping force pulling the dumbbell against viscous drag is shown in red

Detection of more transient interactions in the three-bead assay is made possible by the development of ultrafast force-clamp (UFFC) spectroscopy [44, 50]. To implement UFFC, optical tweezers are used to move the dumbbell beads at a constant velocity (Fig. 1c). The direction of the force is switched periodically, leading to triangular motion of the MT dumbbell (Fig. 1d). When a filament binds to a pedestal-immobilized molecule, the force that is applied to the dumbbell beads is transferred to the molecule. For interactions between myosin and actin, the transfer time between formation of actin–myosin binding and force application is ~10 μs [44]. Factors that decrease the temporal resolution include compliance of the dumbbell bead–filament system, which may cause underestimation of the binding duration and of possible displacements resulting from conformational changes of the protein [51]. Another factor that can degrade measurement accuracy is shakiness of the pedestal; accordingly, it is essential to achieve firm immobilization of the pedestal beads that supports a range of pulling forces.

The UFFC method has thus far been applied to study static and gliding interactions of the actin-binding proteins α-catenin [52] and myosin [44, 53–55], as well as the DNA-binding LacI repressor [44, 56]. However, studies of MAPs are lagging. Although the general optical setup could be the same for different filamentous structures, several features of the MAP-MT system can complicate application of this approach. First, an MT has a significantly higher rigidity (~10^{-23} N · m^2) than actin (~10^{-26} N · m^2) or DNA (~10^{-28} N · m^2) [57]. Because beads are attached laterally to an MT to form a dumbbell, high flexural rigidity is expected to increase overall dumbbell compliance, thereby decreasing time resolution [51]. Second, a common feature of the MAPs is their unstructured charged extensions, which play important roles in MT-dependent diffusional motions. To preserve their full activity, MAP conjugation to the pedestal bead should be stereospecific, providing optimal orientation of these domains relative to the MT.

This chapter describes adaptation of UFFC to investigate force-dependent binding between MAPs and MTs. We describe the design of the major optical components of our instrument and procedures for preparing assay components, including functionalization of pedestal surface. Although our approaches were developed for studying MAPs that connect kinetochores to spindle MTs, these methods should also be useful for studying other MT-binding protein complexes, such as those involved in cortical MT attachments.

2 Materials

2.1 Laser-Tweezers Instrument for UFFC Assay

2.1.1 Microscope and Other Parts

1. Zeiss AxioImager.Z2 microscope.
2. Andor iXon 3 electron-multiplying charge-coupled device (EMCCD) camera.
3. Trapping laser: 1064 nm fiber laser (IPG Photonics, YLR-10-1064-LP).
4. Tracking lasers:
   (a) 780 nm fiber-coupled laser (35 mW, iFLEX 2000, Qioptiq).
   (b) 830 nm fiber-coupled laser (50 mW, iFLEX 2000, Qioptiq).
   (c) 905 nm laser (50 mW, TECIR-50GC-905, World Star Tech).
5. Acousto-optic deflector (AOD) (IntraAction Corp., DTD-274HA6 2-AXIS) with AOD-driver (IntraAction Corp., DE-271).
6. Two quadrant photodetectors (QPD, custom-made).

7. Differential amplifier (frequency range 0–100 kHz, custom-made).
8. Piezo-driven mirror (Physik Instrumente, S330).
9. Actuator-driven gimbal mirrors (Newport, VGM-1N).
10. 530 nm LED-illumination lamp for DIC imaging (Thorlabs, M530D3).
11. 488 nm laser for GFP imaging (Coherent, Sapphire 488-20/460-CDRH).
12. A mercury arc lamp for imaging in the rhodamine fluorescence channel (Zeiss, HBO 100).
13. Filter cubes (Semrock, GFP-3035C-ZHE-ZERO and mCherry-B-ZHE-ZERO).
14. 1.0 OD neutral density filters (Thorlabs).
15. High-speed shutter (Melles Griot, 04UTS201).
16. Single-band band-pass filters (Semrock, FF01-780/12-25 and similar Brightline filters).
17. Polarizing cube beam splitter (Newport, 05FC16PB.5).
18. Actuators (Thorlabs, Z806).
19. Microscope objective thermostat (Bioptechs, R5).
20. Condenser lens thermostat (optional).
21. MetaMorph image acquisition and analysis software.

2.1.2 Stage Stabilization

1. Three-axis piezoelectric stage (Physik Instrumente P-561.3DD).
2. Tracking laser (905 nm, 50 mW, World Star Tech, TECIR 905).
3. One QPD.

2.1.3 UFFC Feedback Regimes

1. One or two AODs depending on the regime.
2. Two QPDs.

2.1.4 Data Transfer Layout

1. Mid-range personal computer (PC) with a 64-bit processor 2.4 GHz or higher, at least 16 GB of RAM and 256 GB SSD, and two slots for data acquisition boards.
2. Field-Programmable Gate Array (FPGA) (National Instruments, PCIe-7842R).
3. Data acquisition connector block (National Instruments, SCB-68).
4. Data acquisition board (National Instruments, PCI-6070E).
5. LabVIEW software (National Instruments).

2.2 Pedestal Bead Immobilization

1. Ultrasonic bath (Branson, 71020-MTH).
2. Microcentrifuge (Eppendorf, 5415R).
3. Vortex (Scientific Industries, 155580).
4. Plasma cleaner (Harrick Plasma, PDS-32G).
5. Heater (Corning PC400D).
6. Polished metal plate (2–3 cm thick).
7. Thermometer thermocouple (Digi-sense, 8528-20).
8. Compressed nitrogen.
9. 1.87 μm streptavidin-coated polystyrene beads (Spherotech, SVP-15-5). This stock solution is stored at 4 °C.
10. 22 × 30 mm glass coverslips (VWR, 48366-067).
11. 22 × 30 mm silanized glass coverslips.
12. 25 × 75 × 1 mm micro-slides (VWR).
13. Double-sided sticky tape (Scotch, 504829).
14. Filter paper (Whatman, WHA10300012).
15. 100 mM sodium acetate trihydrate (Sigma, S8625-250G). This solution is filter sterilized and stored at 4 °C.
16. MgBRB80 Buffer: 80 mM K-Pipes pH 6.9, 1 mM EGTA, and 4 mM $MgCl_2$. This buffer is filter sterilized and stored at 4 °C for several weeks or at −20 °C for longer period.
17. Bovine serum albumin (BSA) (Sigma-Aldrich, A7638). This reagent is prepared at 100 mg/mL in MgBRB80 Buffer, centrifuged at 16,100 × *g* for 15 min at 4 °C to remove aggregates and stored as 100-μL aliquots at −80 °C.
18. Dithiothreitol (DTT) (Thermo Fisher Scientific, 15508). This reagent is prepared at 1 M, filter sterilized and stored as 10-μL aliquots at −80 °C.
19. Phosphate buffered saline (PBS): 140 mM NaCl, 2.7 mM KCl, 10.1 mM Na_2HPO_4, and 1.8 mM KH_2PO_4, pH 7.2. This buffer is filter sterilized and stored at 4 °C for several weeks or at −20 °C for longer period.
20. Incubation Buffer: PBS with 2 mg/mL BSA and 2 mM DTT. This and other buffers with DTT are used for not longer than 4 h after adding DTT.

2.3 Pedestal Bead Functionalization

2.3.1 Functionalization of Pedestals Using SNAP-GBP

1. Biotinylated benzylguanine (biotin-BG) (NEB, S9110S). This reagent is prepared at 100 μM in DMSO and stored as 5-μL aliquots at −80 °C.
2. SNAP-GBP linking protein, which contains a fusion of SNAP-tag (New England Biolabs) and GFP-binding protein (GBP, RCSB Protein Data Bank accession number 3OGO). SNAP-GBP can be expressed in E. coli and purified as in [37].

3. Biotinylated polyethylene glycol (dPEG®$_{48}$-biotin acid) (Quanta Biodesign, 10776). This reagent is prepared at 40 mM in MgBRB80 Buffer and stored as 5-μL aliquots at −80 °C.
4. 1% Pluronic (F127, Sigma, P2443). This reagent is prepared at 10 mg/mL in PBS, centrifuged at 16,100 × *g* for 15 min to remove aggregates and stored as 1-mL aliquots at room temperature for no longer than 2 weeks.

2.3.2 Coating Pedestals with Biotinylated Anti-GFP Antibodies

1. Biotinylated anti-GFP antibodies (Abcam, ab6658). This reagent is prepared at 0.5 mg/mL in 50% glycerol and stored as 30-μL aliquots at −20 °C.
2. Biotinylated BSA (Sigma, A8549-10MG). This reagent is prepared at 225 μM and stored as 10-μL aliquots at −80 °C.

2.3.3 Recruitment of GFP-Tagged MAPs

1. GFP-tagged MAP of interest.
2. Optima MAX-TL Series Benchtop Ultracentrifuge.
3. Beckman TLA-100 rotor.

2.4 Microtubule Dumbbell Preparation

2.4.1 Preparation of MTs

1. Unlabeled porcine tubulin (Cytoskeleton, T240-A).
2. Rhodamine-labeled porcine tubulin (Cytoskeleton, TL590M-A).
3. TAMRA Succinimidyl Ester (ThermoFisher, C1171), stored at −20 °C.
4. Digoxigenin (DIG) Succinimidyl Ester (ThermoFisher, A2952), stored at −20 °C.
5. GTP (Sigma-Aldrich, G8877). This reagent is prepared at 50 mM in 50 mM $MgCl_2$, pH adjusted to 7.0 with NaOH, and stored as 10-μL aliquots at −80 °C.
6. Paclitaxel (taxol) (Sigma-Aldrich, T7402). This reagent is prepared at 1 mM in DMSO and stored as 10-μL aliquots at −80 °C.
7. Glycerol (MP Biomedical, 02151194-CF).

2.4.2 Preparation of Dumbbell Beads Coated with Anti-Tubulin Antibodies

1. Streptavidin-coated polystyrene beads 0.54 μm diameter (Spherotech, SVP-05-10), stored at 4 °C.
2. Biotinylated anti-tubulin antibodies (Biolegend, 801212). This reagent is diluted with 50% Glycerol and stored at −20 °C.

2.4.3 Preparation of Dumbbell Beads Coated With Anti-DIG-Antibodies

1. Carboxylated polystyrene beads 0.48 μm diameter (Spherotech, CP-05-10), stored at 4 °C.
2. Sulfo-NHS (Sigma, 56485), stored desiccated at −20 °C.

3. 1-Ethyl-3-(3-dimethylaminopropyl) carbodiimide hydrochloride (EDC) (Thermo Fisher Scientific, 22980), stored desiccated at −20 °C.
4. Glycine (Fisher, BP381). This reagent is diluted to 1 M in PBS and stored at −80 °C.
5. MES.TWIN Buffer: 25 mM MES + 0.05% TWIN, pH 5.0. This buffer is filter sterilized and stored at 4 °C for several weeks or at −20 °C for longer period.
6. Anti-DIG Fab fragments (Roche, 11 214 667 001). This reagent is diluted to 1 mg/mL in PBS supplemented with 30% glycerol and stored at −20 °C.
7. Storage Buffer: PBS with 7 mg/mL BSA and 1 mM DTT.

2.5 Ultrafast Force-Clamp Assay

2.5.1 Preparation of Chamber with Functionalized Pedestals and MT

1. Glucose (Sigma-Aldrich, G8270). This reagent is prepared at 600 mg/mL in Milli-Q water and stored as 10-μL aliquots at −80 °C.
2. Glucose oxidase (Sigma-Aldrich, G2133). This reagent is prepared at 10 mg/mL in Milli-Q water and stored as 10-μL aliquots at −80 °C.
3. Catalase (Sigma-Aldrich, C40). This reagent is prepared at 8 mg/mL in Milli-Q water and stored as 10-μL aliquots at −80 °C.
4. 2-Mercaptoethanol (BME) (Sigma-Aldrich, M3148). This reagent is stored in 5-μL aliquots at −80 °C.
5. Assay Buffer: MgBRB80 Buffer supplemented with 4 mg/mL BSA, 2 mM DTT, 0.01 mM taxol, 0.5% BME, 6 mg/mL glucose, 0.1 mg/mL glucose oxidase, and 0.8 mg/mL catalase.
6. Kwik-Cast Sealant (World Precision Instruments, KWIK-CAST).

3 Methods

3.1 Laser-Tweezers Instrument for UFFC Assay

Optical tweezers are often constructed based on an inverted light microscope. Our system includes the upright microscope configuration, which is preferable when working with beads coated with dense protein coats: such beads tend to clump, but in the upright microscope, bead aggregates sink quickly to the bottom of the microscopy chamber, leaving the upper coverslip free from bead clumps and debris. Another advantage of the upright configuration is that it permits a more straightforward incorporation of laser beams without sacrificing differential interference contrast (DIC) and epifluorescence imaging capabilities [58]. We custom-modified a Zeiss AxioImager microscope to increase its mechanical stability

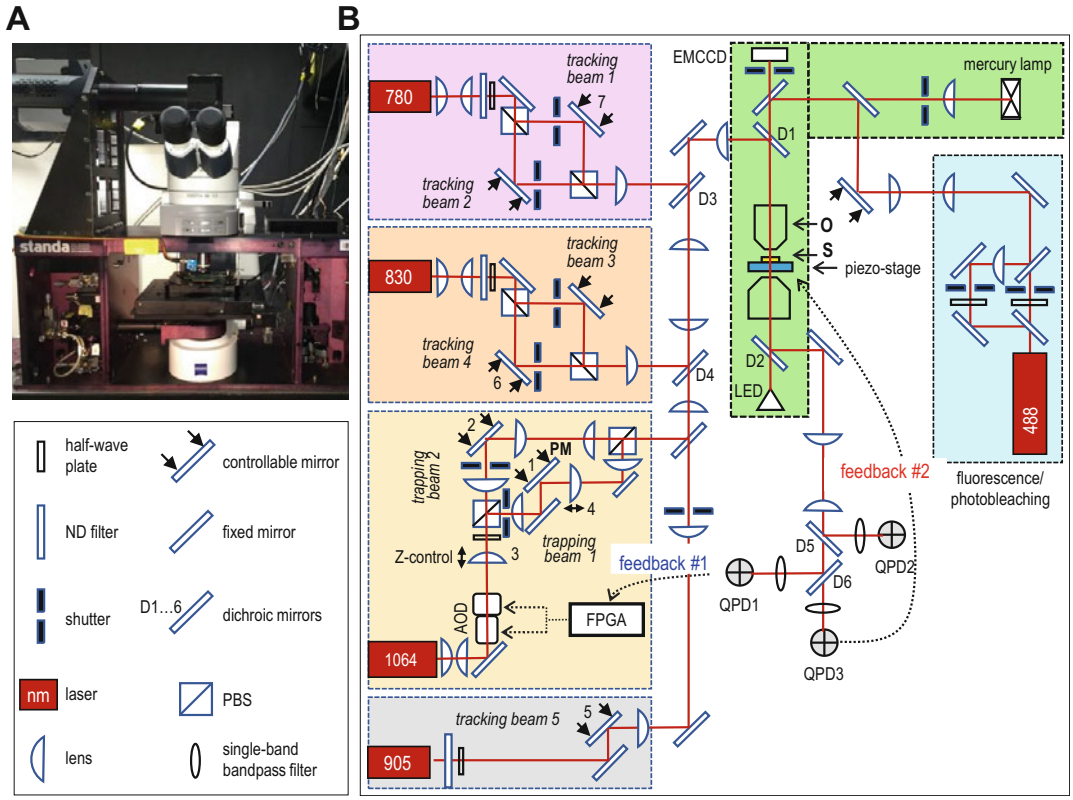

Fig. 2 Laser-tweezers instrument. (**a**) Photograph of our microscope accommodating the UFFC system. (**b**) The optical microscope system consists of the following components: DIC pathway including light emitting diode (LED), condenser, polarizers and Wollaston prisms (not shown); sample (S), *x,y,z* piezo-stage, objective (O), and EMCCD. Dual optical tweezers are inserted and extracted from the optical axis of the microscope through dichroic mirrors (D1 and D2) and comprise: Ytterbium laser (1064 nm), half-wave plates, polarizing beam-splitter cubes (PBS), AOD and piezo-mirror (PM). Two tracking beams are aligned with two trapping beams, and the third tracking beam is projected through a pedestal bead. Dichroic mirrors D5 and D6, and three QPDs distribute beams and acquire information about dumbbell and pedestal beads. *Tracking beam 4* (830 nm) coupled with *QPD1* monitors position of bead 1 in TRAP1. *Tracking beam 1* (780 nm) coupled with *QPD2* monitors position of bead 2 in TRAP2. *Tracking beam 5* (905 nm) coupled with *QPD3* monitors position of pedestal bead and provides feedback #2 for stage stabilization. Signals from *QPD1* and *QPD2* are processed with an FPGA and sent to the AOD controller to implement UFFC feedback #1

(Fig. 2a) and to incorporate the trapping and tracking beams, as well as QPD detection system [47, 59]. This instrument was subsequently upgraded for UFFC spectroscopy using the general optical layout for dual trapping described in [60]. Additionally, our instrument features three-axis piezo-stage mediated feedback system to decrease stage drift, and it incorporates multifunctional field-programmable gate array (FPGA) for data acquisition, force feedback calculations and optical traps control. The recommendations for setting up a laser-tweezers system suitable for the UFFC assay are detailed below.

3.1.1 Microscope and Other Paths (Fig. 2b)

1. For improved mechanical stability, the microscope and other optical elements should be situated on an optical table in a room with a controlled environment, maintaining the temperature at 20 °C. All optical paths should be minimized in length and enclosed to reduce the influence of air fluctuations, permitting measurements of 0.1–50-pN forces with characteristic times ranging from 0.5 ms to a few hours.
2. The microscope incorporates a 100× 1.46 NA oil objective, a 488-nm laser and mercury lamp for fluorescence excitation, and a high-speed shutter to decrease photobleaching.
3. A three-axes piezo-stage provides fine movement of the sample with nanometer precision. The piezo-stage is mounted on a motorized *x,y* stage, which is used for coarse positioning.
4. A 10-W linearly polarized continuous wave ytterbium laser at a wavelength of 1064 nm is used for optical trapping. After collimation, the laser beam passes through a dual-axis acousto-optic deflector (AOD) (*see* **Note 1**).
5. After a half-wave plate, a polarizing beam-splitter cube splits the beam into *trapping beams 1* and *2* (Fig. 2b). These beams are expanded separately using a pair of beam expander lenses in telescopic mode. The beams are then combined using a second polarizing beam-splitter cube. With the help of dichroic mirrors, the beams are directed into the microscope and focused by the objective lens to create two traps.
6. Adjustment of the *x,y* position of *trapping beam 2* is performed independently of *trapping beam 1* using an actuator-driven gimbal *mirror 2*. This control is needed to develop pre-tension on the MT dumbbell during the UFFC assay. The position of *trapping beam 1* is adjusted via *x,y* piezo-driven *mirror 1*.
7. The focus of both trapping beams can be adjusted simultaneously, or the beams can be focused independently, using *lenses 3* and *4*. The lenses are installed on actuators controlled with a custom program written in LabVIEW.
8. Position detection of each trapped bead is accomplished through back-focal-plane detection of light from two fiber-coupled lasers: *tracking beam 1* (780 nm) and *tracking beam 4* (830 nm) (*see* **Note 2**). The intensities of these lasers are reduced using 1.0 OD neutral density filters.
9. After the light from a tracking beam becomes scattered by a bead held in the corresponding trapping beam, it is collected by the condenser lens, redirected, and focused onto the corresponding QPD. Single-band band-pass filters are placed in front of each QPD to decrease crosstalk between the two beams. Signal from each QPD quadrant is amplified and passed

through a differential amplifier. This supplies normalized *x*- and *y*-position signals and a third signal that represents their sum and corresponds to the *z*-coordinate,

10. In optical tweezers utilizing dedicated tracking beams, each tracking and trapping beam pair and the corresponding QPD should be aligned and calibrated every time a bead is captured into a trap. Fine adjustments of *tracking beams 1* and *4* are carried out using corresponding actuator-driven gimbal mirrors *(mirrors 7* and *6* in Fig. 2b). To align the tracking and trapping beams, these mirrors are used to bring the *x*- and *y*-readings of the corresponding QPDs to zero. Then, AOD crisscross calibration is carried out by instructing AOD to move each trapped bead along *x* and *y* directions with a 10-nm step from −0.5 to 0.5 μm [59]. The measured QPD voltage response is fitted with a seventh-order polynomial, and the fitting coefficients are used to convert the bead position from voltage to nanometers and to obtain the dumbbell bead's displacement during the experiment.
11. To determine stiffness of a trap, a captured bead is monitored with QPD at 20 kHz for 1 s consecutively 30 times and the averaged power spectrum is fitted with Lorentzian [61].

3.1.2 Stage Stabilization

1. Stage drifts are minimized using a computer-controlled feedback system (*feedback #2,* Fig. 2b). This system utilizes *tracking beam 5* from a 905 nm laser, a coverslip-immobilized pedestal bead and a dedicated QPD (*QPD3* in Fig. 2b).
2. For proper stage stabilization, the pedestal, *tracking beam 5* and *QPD3* should be aligned. Start by confirming that there are no pedestals or any other objects in the experimental chamber in the vicinity of the tracking beam. Mark position of *tracking beam 5* on the imaging window on a computer screen using any drawing tool. To align *tracking beam 5* and *QPD3*, adjust the position of *QPD3* to zero the *x*- and *y*-axis signals. Confirm that the *z*-axis signal is not zero, indicating that the light from the tracking beam is projected onto the QPD. Using the coarse stage controls and then the piezo-stage, bring one of the immobilized pedestals to match its center with the mark on the screen.
3. Calibrate *QPD3* by moving the pedestal bead along the *x*, *y*, and *z* directions with the piezo-stage (stage crisscross calibration). This calibration is identical to the AOD crisscross calibration except the bead motion is driven by the piezo-stage.
4. To implement stage stabilization program, collect pedestal's (*x*, *y*,*z*) coordinates at 1 kHz via data acquisition board. Every 10 frames are averaged and used to generate a signal, which is proportional to the measured displacement for every axis. The error-correction signal is then sent to the piezo-stage controller to adjust the piezo-stage position.

3.1.3 UFFC Feedback Regimes

In the UFFC assay, an MT dumbbell is first stretched to exert pre-tension F_0. It is then moved against viscous drag in the buffer under constant force F by two synchronous traps in a triangular-wave fashion (Fig. 1d). To implement the force clamp, different feedback regimes can be used, depending on the available equipment and specific experimental goals. The original study by Capitanio and colleagues [44] used an optical system in which two AODs control two independent optical traps (Fig. 3a). With this configuration, two separate feedback loops maintain different displacements (and therefore force) for the "leading" and "trailing" dumbbell beads, which are located at the front and back of the moving dumbbell, correspondingly. Specifically, the position of the leading trap is adjusted to clamp the leading bead displacement to exert force $F + F_0$, whereas the position of the trailing trap is adjusted to maintain displacement of the trailing bead corresponding to the pre-tension force F_0. Every time the dumbbell changes its direction of motion, the trailing bead becomes leading, resulting in an identical force regime for both directions (Fig. 3a).

In the laser-tweezers instrument featuring a single AOD and two optical traps derived from the same parental beam, these traps are naturally synchronized. This is advantageous because angular fluctuations of the trapping beams are a major source of signal noise, and when two independent laser traps are used, the resultant noise is additive. However, in dual traps derived from the same parental beam these fluctuations are synchronized, and the distance between the trapped beads is well maintained. With this optical scheme, the force clamp can be implemented using a single feedback loop. In the "leading trap feedback" regime, two tracking beams and their corresponding QPDs are involved in actively clamping the force only for the leading bead (Fig. 3b). Signal from the QPD that monitors the leading bead is used to adjust the position of the leading trap, such that its displacement corresponds to the sum of the pre-tension force F_0 and force $F/2$, where F is the input clamped force for the dumbbell. Because the distance between two traps is constant due to the design of the optical path, the force acting on the trailing bead is $F/2 - F_0$, generating the total force F on the dumbbell.

An even simpler single–feedback loop regime can be implemented by clamping the same bead regardless of whether it is leading or trailing ("same trap feedback," Fig. 3c). Although the distribution of forces acting on the dumbbell beads is the same as in the "leading trap feedback" regime, signal noise is noticeably higher when the force is clamped using the trailing bead's position, because it has on average a smaller displacement from the trap's center than the leading bead. This noise asymmetry is the most significant drawback of the otherwise straightforward feedback scheme, which employs only one tracking beam and one QPD.

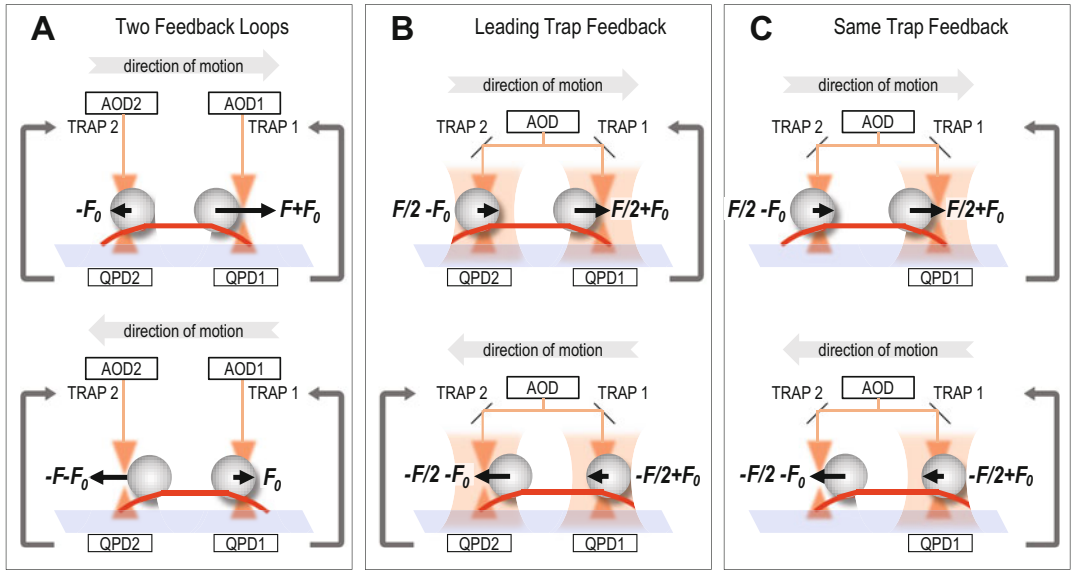

Fig. 3 Operational principles of the UFFC feedback loops. (**a–c**) Schematics for different regimes to exert control of the trap(s) position in response to changes in the position of dumbbell bead(s), as determined with QPD(s). With all regimes, the MT dumbbell stretched with force F_0 is oscillated under constant force F, but the regimes differ in the noise level for signals collected from different beads (see text for more details). More narrow and darker cones depict trapping beams, whereas tracking beams are depicted with wide cones and light color

3.1.4 Data Transfer Layout

Force feedback in the desired regime is realized via firmware programmed into a memory of FPGA. The firmware carries out on-board processing of digitized data from QPDs and generates a correction signal for AOD. The FPGA board installed in a PC is wired to the outputs of QPD differential amplifiers and to the input of the AOD-driver through the data acquisition connector block (Fig. 4a).

1. To implement a force feedback loop, use a custom-written LabVIEW program to send calibration coefficients and stiffness for both laser traps to the FPGA board's memory. Also, input the desired force value to be maintained by the clamp.
2. After the force-clamp is initiated, the FPGA digitizes signals from differential QPD amplifiers and calculates the current position of a dumbbell bead using the input calibration coefficients. Updated trap position is then calculated, and the corresponding analog voltage signal is sent to the AOD to steer the trapping beam. The coordinates of the dumbbell beads and optical traps are transferred to a data file on the PC.
3. QPD signals are acquired and processed by FPGA to generate an AOD control signal every 15 μs (66 kHz). The feedback delay time can be measured by sending a control signal from the FPGA and detecting the resultant change in trap's position

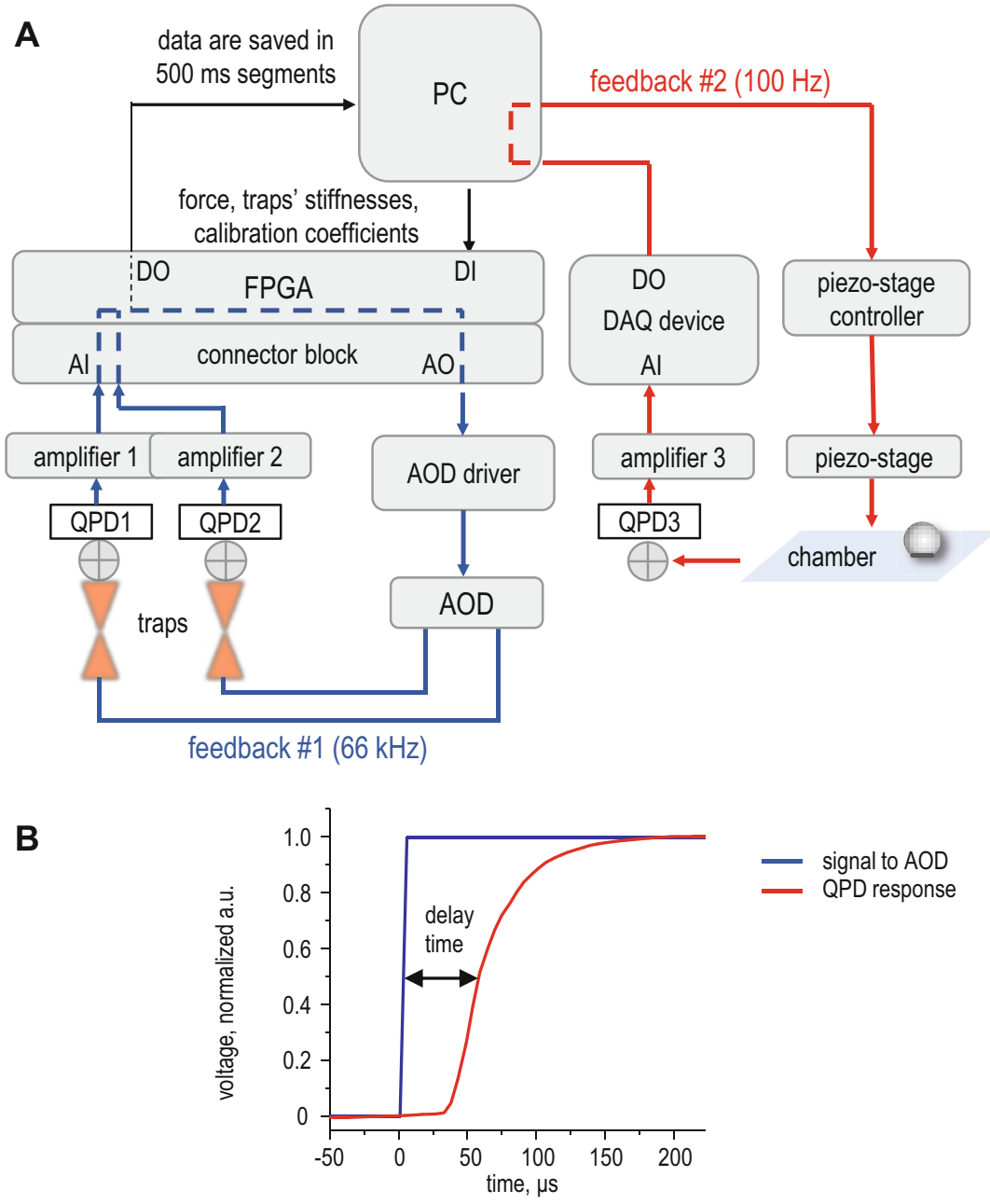

Fig. 4 Data transfer layout for feedback loops. (**a**) Our instrument is controlled with two feedback loops, in which data are transferred in the directions depicted with arrows. Blue arrows represent the force-clamp feedback loop, red arrows represent the stage stabilization feedback loop. *AI* analog input, *AO* analog output, *DI* digital input, *DO* digital output. (**b**) Blue curve shows the step-like signal generated by the FPGA to instruct the AOD to sweep the trapping beam across a coverslip-immobilized pedestal. The resultant QPD response signal (red curve) reveals instrument delay

with the QPD. In our system, this delay time is ~60 μs (Fig. 4b), which is comparable with estimated delay times in other published studies [44, 54].

3.2 Pedestal Bead Immobilization

For successful implementation of the UFFC assay, the pedestal beads must be firmly immobilized to support forces that arise when a pedestal-bound MAP molecule interacts with a dumbbell MT. Additionally, pedestals should be functionalized to ensure specific recruitment of MAP molecules and their proper orientation, in which MT-binding domains are facing away from pedestal surface. A common method to immobilize pedestal beads is to coat them with nitrocellulose, which "glues" pedestals to the coverslip surface [62]. However, this approach does not provide specific orientation of conjugated molecules because proteins are recruited through nonspecific adhesion to nitrocellulose. We also found that some proteins, such as the MT-binding Ndc80 complex [63], bound strongly to nitrocellulose coating, presumably because negative electric charges of the nitrocellulose [64] interact with positively charged extensions and amino acid patches within the MT-binding domains of the Ndc80 complex [65]. Because positively charged residues are a common feature of the MT-binding proteins, recruitment via nitrocellulose could prevent these proteins from normal interactions with the MTs. To circumvent this problem, we developed two different methods for preparing stable and functionally active pedestals. Both methods use commercial streptavidin-coated polystyrene beads. In the first method, the beads are heated briefly to cause their partial melting. In the second, the beads adhere to the coverslip nonspecifically. Below, we describe pedestal bead immobilization procedures, as well as methods for testing the stability of pedestal immobilization (*see* Subheading 3.3). Subsequently, the immobilized pedestals are coated with anti-GFP antibodies or with SNAP-GBP linker, enabling recruitment of different GFP-labeled MAPs (*see* Subheading 3.4).

3.2.1 Partial-Melting Method

When the glass coverslip is heated briefly, polystyrene beads will melt at the site of their contact with the coverslip. Such partial melting has the potential to provide utmost stability for pedestal beads. This method requires a highly optimized temperature regime, such that the bead melts only at the site of contact with the coverslip. Streptavidin is thermally stable up to 75 °C, and soluble streptavidin loses its tetrameric structure when heated for 3 min at 90 °C [66]. Thus, the temperature and duration of melting should be chosen to attach the pedestal beads to the coverslip while maintaining their spherical shape and the functionality of streptavidin on their surfaces.

1. Regular glass coverslips should be cleaned in a ceramic/glass rack in a plasma cleaner for 10 min at 30 W.

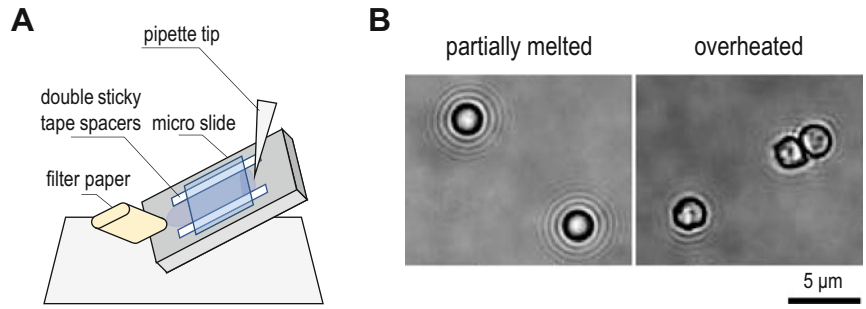

Fig. 5 Immobilization of pedestals. (**a**) Schematic of the microscope chamber and application of flow by gravity. (**b**) Bright-field images of streptavidin-coated beads 1.87 µm diameter. Proper heat application results in partial bead melting, which firmly immobilizes beads on the coverslip while preserving the spherical shape of bead surface that was not in direct contact with the heated glass. Excessive heating leads to visible loss of spherical bead shape, resulting in immobilized but unusable pedestals

2. To achieve uniform heating throughout the coverslip, a polished metal plate is placed on top of a lab heater. Set the heater at 160 °C and preheat the metal plate for 1 h. Temperature at the upper surface of the plate will rise to ~100 °C, as measured with a thermocouple thermometer.
3. Vortex stock solution of 1.87-µm streptavidin-coated polystyrene beads for 20 s.
4. Dilute stock bead suspension ten-fold in 100 mM sodium acetate trihydrate.
5. Sonicate diluted beads for 10 s in an ultrasonic bath filled with iced water.
6. Add 2 µL of diluted bead solution as a drop at one end of a 22 × 30 mm coverslip and spread the beads with a clean glass micro-slide (*see* **Note 3**). Repeat this procedure to prepare 3–5 coverslips.
7. Let the coated coverslips dry for at least 5 min at room temperature.
8. Using metal tweezers, place one coverslip in the middle of the hot metal plate for 10 s. Because the duration of heating is critical, use a lab timer and heat one coverslip at a time (*see* **Note 4**).
9. Let the coverslips cool for 5 min at room temperature.
10. Wash thoroughly with Milli-Q water, holding the coverslips parallel to the direction of water flow to remove salt deposit and unmelted beads.
11. Dry the coverslips by blowing compressed nitrogen over them.
12. Immediately prepare three flow chambers using coverslips with immobilized pedestals, clean micro-slides and double sticky tape spacers (Fig. 5a). Flow 20 µL of Incubation Buffer into

each chamber. Use one chamber immediately and store other chambers at room temperature in a closed container with moist paper towel (*see* **Note 5**). Discard unused chambers and coverslips at the end of UFFC experiment.

13. Inspect the pedestal beads by DIC imaging to verify the density and shape of partially melted beads (Fig. 5b).
14. Proceed with bead functionalization as described in Subheading 3.4.

3.2.2 Adsorption Method

In this approach, streptavidin-coated polystyrene beads nonspecifically adhere to recently silanized coverslips (prepared within 1 week) (*see* **Note 6**). To avoid mechanical damage to the silanized surface, these coverslips should be handled by holding onto the corners with forceps, and they should be stored in a box wrapped with ultrasoft tissue paper, making sure that the coverslips do not overlap with each other.

1. Prepare flow chambers of approximate volume 15–20 μL using one silanized coverslip, one 25 × 75 × 1 mm micro-slide, and double sticky tape spacers (Fig. 5a).
2. Vortex 1.87 μm streptavidin-coated polystyrene beads stock for 20 s.
3. Resuspend 1 μL bead stock in 100 μL PBS. Centrifuge at 10,000 × *g* for 8 min at 4 °C, and resuspend beads in 200 μL PBS.
4. Flow 20 μL of bead solution into the chamber, flip the chamber to keep the coverslip down, and incubate for at least 40 min at room temperature. Longer incubation (up to 2 h) results in stronger bead adhesion.
5. Wash the chamber gently using gravity flow: keep the microslide in an angled position, carefully add 50 μL of PBS on one side of the chamber and let the liquid flow under the force of gravity (Fig. 5a). Slowly remove excess liquid using filter paper.
6. Incubate pedestals in PBS for 5 min and wash the flow chamber again as in **step 5** above.
7. Flow 20 μL of Incubation Buffer into the chamber. Proceed with bead functionalization as described in Subheading 3.4.

3.3 Testing the Strength of Pedestal Immobilization

When properly executed, the partial-melting method provides very firm bead–coverslip attachment. However, insufficiently high temperature can lead to loosely attached pedestals. The adsorption method may also produce insufficiently strong immobilization, as variable stability of pedestals is often observed on the same coverslip or in samples prepared on different days. To evaluate the strength of immobilization for individual pedestals and their suitability for UFFC, we use two methods: monitoring thermal vibrations of pedestals and pulling pedestal beads with the laser trap.

3.3.1 Monitoring Thermal Vibration (Standard Deviation (SD) Method)

Firmly immobilized pedestal beads should exhibit virtually no thermal vibration, whereas loosely attached pedestals experience small rocking. Such motions may be invisible during microscopy-assisted visualization, but they are readily detected by QPD monitoring and quantified using the SD of pedestal position.

1. Take a freshly prepared chamber with immobilized pedestals and flow 50 μL of PBS prewarmed to 37 °C.
2. Calibrate QPD (*QPD 3* in Fig. 2b) using the stage crisscross calibration procedure.
3. Record the pedestal bead's position for 20 s at 1 kHz acquisition rate, and calculate the SD using a 100-ms sliding window (Fig. 6a–c).
4. Figure 6d shows the typical distributions of SDs for thermal vibration of individual pedestals immobilized via partial melting and adsorption, as well as for a control pedestal attached loosely onto the coverslips (red curve). Nonspecific adsorption produces pedestals with excellent average stability, comparable to that of partially melted beads (Fig. 6e). However, SDs of individual adsorbed pedestals exhibit considerable variability (Fig. 6f). To avoid collecting data with shaky pedestals, prior to force-clamp measurement each pedestal should be examined using the SD-based method. We recommend collecting UFFC data only with pedestals that have SD < 5 nm, as described in Subheading 3.6.5.

3.3.2 Pulling Pedestal Beads via Optical Trap

In the three-bead optical-tweezers assay, considerable forces arise upon binding between the pedestal-conjugated MAP molecule and dumbbell MT. Such forces may result in tilting of the pedestals, leading to measurement errors. The strength of pedestal immobilization can be tested by oscillating the trapping laser beam focused on a pedestal (*see* **Note 7**).

1. Use 0.5 μL of 1.8 μm streptavidin–coated polystyrene beads to dilute 1000-fold in PBS prewarmed to 37 °C.
2. Flow 50 μL of diluted beads into a freshly prepared chamber with immobilized pedestals.
3. For control measurement, trap a floating 1.8 μm bead in one of the laser beams and calibrate the corresponding QPD using AOD crisscross calibration.
4. With AOD, oscillate the trapped bead sinusoidally for 30 s with amplitude 200 nm at 10 Hz, and record the bead position at the 50-kHz acquisition rate. Perform Fourier transformation of these data using MATLAB or OriginLab. Fourier-transformed data for control beads will show a peak at 10 Hz (Fig. 7a).

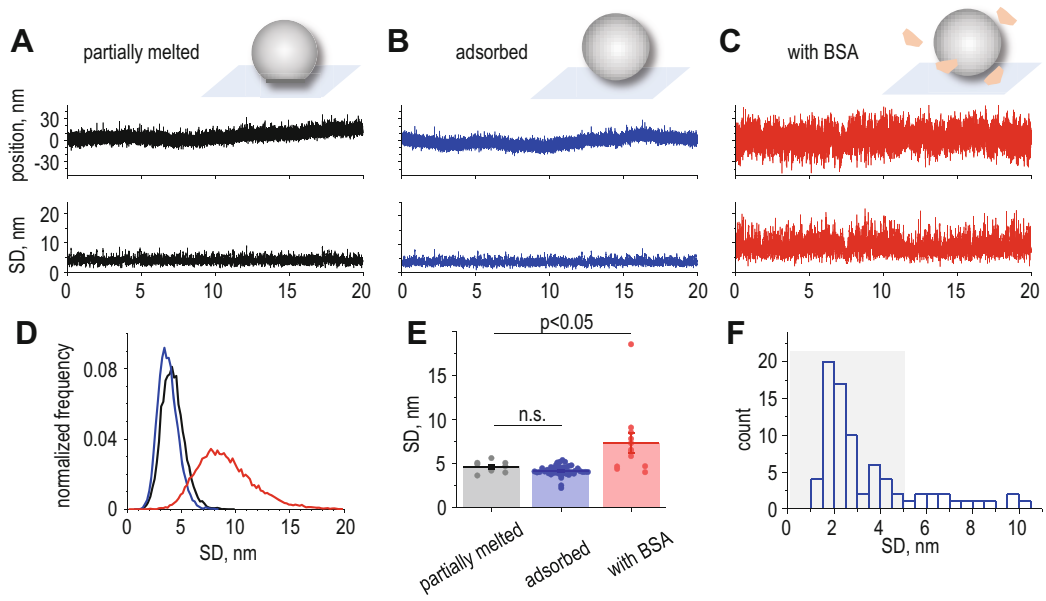

Fig. 6 SD method for testing stability of immobilized pedestals. (**a–c**) Representative QPD signals for pedestal bead coordinates and running SDs (100 ms window) along *y*-axis, which in our system aligns with the MT dumbbell. Loosely attached pedestals are obtained via nonspecific adsorption in the presence of 8 mg/mL BSA (*see* **step 4** in Subheading 3.2.2). (**d**) Example distributions of the running SDs for three types of pedestals are depicted using the same color coding as in panels A–C. (**e**) Pedestal SDs. Each dot shows average SD for one pedestal immobilized using indicated procedures. Bars with errors correspond to means ± SEM, *p*-value determined by Mann–Whitney test. (**f**). Histogram plot of the SDs of adsorbed pedestals shows considerable variability in pedestals stability (data from nine chambers, examining total 87 pedestals). Gray area shows pedestals with SD $<$ 5 nm, which was chosen as a cutoff to select firmly attached pedestals for UFFC experiments

5. In the same chamber, find an immobilized pedestal bead and bring the trapping laser beam on top of the pedestal bead. Perform stage crisscross calibration.
6. Repeat the trapping beam oscillations and Fourier transformation as in **step 4**. Well-immobilized pedestals should show no visible changes in bead position and no 10-Hz peak (Fig. 7b).
7. For additional control, prepare a chamber with pedestals attached loosely to the coverslip. Their rocking under the oscillating trap will be clearly visible (Fig. 7c).

3.4 Pedestal Bead Functionalization

The use of streptavidin-coated beads for pedestals enables specific recruitment of proteins via their tags, such as GFP. We recommend using protein constructs in which GFP is located away from the MT-binding domains, decreasing the likelihood that these domains will be masked or hindered from MT association. GFP can be recruited to the pedestals using commercial anti-GFP antibodies or a linking protein that contains a single-chain nano-body (GFP-binding protein, GBP) fused to SNAP-tag, enabling

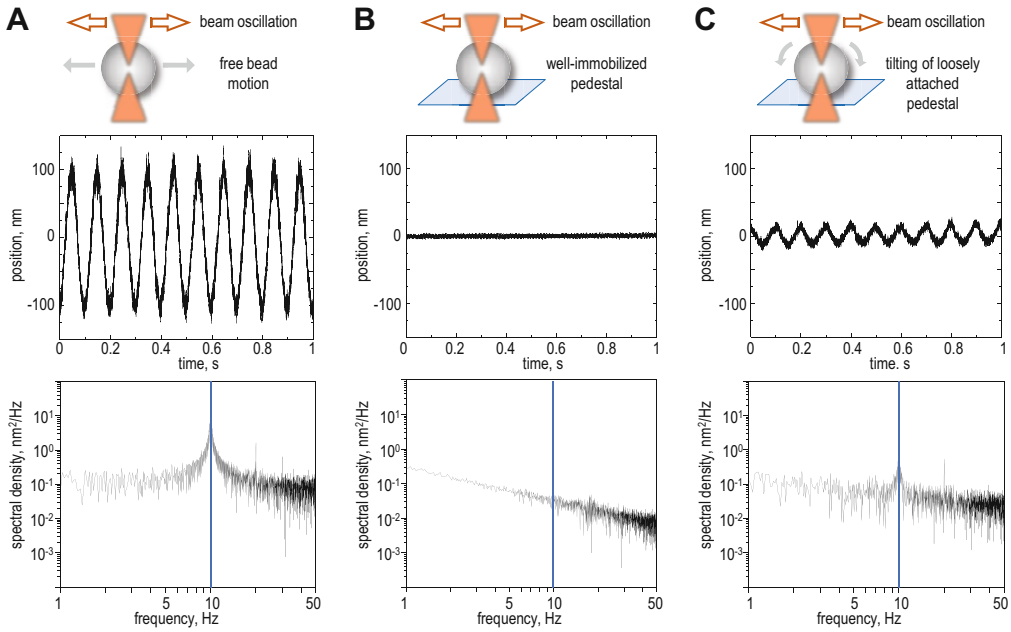

Fig. 7 Testing stability of pedestal immobilization by applying oscillating force. Changes in the coordinate of the bead center and corresponding fast Fourier transformation for streptavidin-coated polystyrene beads (diameter 1.8 μm) subjected to an oscillating laser force with 200-nm amplitude at 10 Hz (blue vertical lines). (**a**) A freely floating bead shows a full range of motion and strong peak at 10 Hz. (**b**) Pedestal immobilized via adsorption shows no detectable motion or distinct frequency. (**c**) Pedestal attached loosely via adsorption in the presence of BSA can be tilted by oscillating laser trap, as seen from periodic changes in its position

straightforward biotinylation [37]. Furthermore, GFP fluorescence is advantageous because it allows monitoring the level of protein coating of pedestals beads, increasing the reproducibility and robustness of the final results (*see* **Note 8**). The conventional approach to ensuring that protein–filament interaction is established via a single molecule is to gather data under conditions in which only a small fraction of pedestals demonstrate interaction [45, 67]. Because of the complexities of the UFFC assay, it is not always possible to collect large statistics from a single experimental chamber, so establishing with confidence the fraction of interacting pedestals in each experiment remains challenging. The brightness of pedestals along with the overall percentage of interacting pedestals collected from different chambers can be used to increase likelihood that the outcome corresponds to a single-molecule regime.

3.4.1 Functionalization of Pedestals Using SNAP-GBP

1. Prepare a mixture of 10 μL of 0.4 μM biotin-BG and 10 μL of 10 μM SNAP-GBP in Incubation Buffer. Pipet well and incubate in the dark for 30 min at 37 °C to biotinylate SNAP-GBP.
2. Take a fresh chamber with pedestal beads immobilized using adsorption method (*see* **Note 9**).

3. Flow the 20-μL mixture prepared in **step 1** into the chamber with pedestals and incubate for 30 min at room temperature.
4. Wash the chamber by flowing the 75 μL Incubation Buffer and incubating for 5 min. Repeat this step.
5. Block all surfaces by flowing 20 μL of 1% Pluronic in Incubation Buffer and incubating for 10 min at room temperature.
6. Wash the chamber as in **step 4**.
7. Block the pedestal surface by flowing 40 μL of 1 mM biotinylated PEG and incubating for 15 min at room temperature (*see* **Note 10**).
8. Wash the chamber as in **step 4**. The chamber is ready to recruit GFP-tagged MAPs, as described in Subheading 3.4.3.

3.4.2 Coating Pedestals with Biotinylated Anti-GFP Antibodies

1. Take a fresh chamber with immobilized pedestal beads.
2. Flow 50 μL anti-GFP antibody diluted to 0.08 μg/mL in Incubation Buffer; incubate for 15 min at room temperature.
3. Wash the chamber by flowing the 75 μL Incubation Buffer and incubating for 5 min. Repeat this step.
4. Block pedestal surface by flowing 40 μL of 1 mM biotin-PEG and incubating for 10 min.
5. Wash the chamber once by flowing the 100 μL Incubation Buffer.
6. Flow 50 μL of 22.5 μM biotinylated BSA and incubate for 10 min.
7. Wash the chamber by flowing the 75 μL Incubation Buffer and incubating for 5 min. Repeat this step.
8. The chamber is ready to recruit GFP-tagged MAPs, as described in Subheading 3.4.3.

3.4.3 Recruitment of GFP-Tagged MAPs

Preparations of purified MAPs often contain small aggregates, which can derail single-molecule measurements. Upon thawing the protein aliquot, aggregates should be removed by ultracentrifugation. Because the extent of protein aggregation varies among protein preparations, this procedure often decreases the soluble protein concentration to a varying degree. Therefore, when accurate control of the density of pedestal coating is desired, the final concentration of MAP solution should be determined for each protein batch or even for each experiment, using spectrophotometry or fluorescence microscopy [68].

1. Dilute freshly thawed protein aliquot in Incubation Buffer to the desired concentration (typically 0.3 μM) and spin in a Beckman centrifuge at 140,000 × *g* for 15 min at 4 °C.

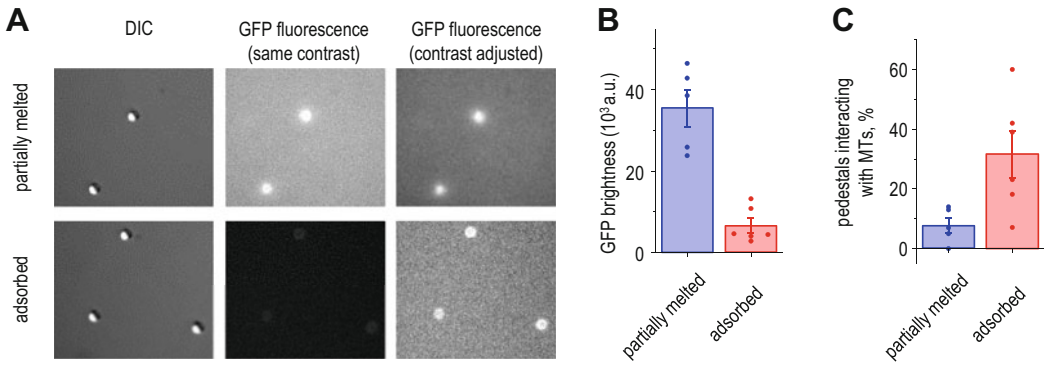

Fig. 8 Coating of immobilized pedestals with GFP-tagged proteins. (**a**) Representative DIC and GFP fluorescence images of functionalized pedestals. Partially melted pedestals were coated with anti-GFP antibodies and 200 nM GFP-tagged protein. Adsorbed pedestals were coated using SNAP-GBP and 10 nM GFP-tagged protein. (**b**) Quantifications of bead brightness and (**c**) percent of pedestals showing interactions with MT dumbbells. Each dot in (**b**) corresponds to the average result from one experimental chamber, in which brightness was collected from >30 pedestals. Each dot in (**c**) corresponds to the result from one experimental chamber in which MT dumbbell interactions were examined for >10 pedestals. Bars with errors are means ± SEM

2. Immediately collect the supernatant, while leaving 10–20 μL of residual solution. Transfer the supernatant into pre-chilled Eppendorf tube and keep on ice for the duration of the experiment. To minimize GFP bleaching, keep protein solution away from light.
3. When ready to use, dilute GFP-tagged protein to the desired concentration in Incubation Buffer.
4. Flow 30 μL of protein solution into the chamber with immobilized pedestals coated with anti-GFP antibodies or SNAP-GBP, as described in Subheadings 3.4.1 and 3.4.2.
5. Incubate for 30 min at room temperature.
6. Wash the chamber by flowing the 75 μL Incubation Buffer and incubating for 5 min. Repeat this step.
7. Flow 50 μL of Assay Buffer prewarmed to 37 °C. Proceed directly to UFFC assay (*see* Subheading 3.6) or examine pedestal coating via fluorescence microscopy. When viewed via GFP fluorescence channel, the pedestals should appear evenly coated and have no bright protein aggregates (Fig. 8). Collect bead brightness to verify that the level of GFP-MAP coating increases linearly at low concentrations of soluble protein (*see* **Note 11**). However, nonspecific binding of protein to pedestal and coverslip surfaces can distort this correlation and affect the fraction of interacting pedestals (*see* **Note 12**).

3.5 Microtubule Dumbbell Preparation

A stable MT dumbbell is essential for accurate UFFC measurements. Unstable attachments cause rupture of the bead–MT connection or lead to a sudden change in MT dumbbell length during the assay. Below, we provide a protocol for forming MT dumbbells using beads coated with anti-tubulin antibodies. Alternatively, the dumbbells can be prepared using MTs polymerized with DIG-labeled tubulin and beads coated with anti-DIG antibodies. In our experiments, most dumbbells prepared using these protocols withstand forces up to 20 pN.

3.5.1 Preparation of Microtubules

MTs can be polymerized using unlabeled porcine tubulin purchased from commercial sources. We recommend including rhodamine-labeled tubulin to assist MT visualization during dumbbell preparation. To prepare DIG-labeled MTs, tubulin can be purified from cow brains [69], and labeled with Digoxigenin Succinimidyl Ester [70]. Rhodamine-labeled bovine tubulin is prepared analogously using TAMRA Succinimidyl Ester.

1. To prepare MTs, mix unlabeled and rhodamine-labeled tubulin at a 12:1 ratio. If DIG-labeled MTs are desired, prepare the same mixture but with DIG-labeled tubulin (*see* **Note 13**).
2. The tubulin mixture can be induced to polymerize in MgBRB80 buffer supplemented with 10% glycerol and 1 mM GTP at 37 °C using any published protocol; we follow the procedure in [68]. Polymerization for 15 min routinely produces MTs with an average length of 9–11 μm (*see* **Note 14**). MTs are stabilized with 10 μM taxol and stored at room temperature in the dark for no longer than 3 days.

3.5.2 Preparation of Dumbbell Beads Coated with Anti-Tubulin Antibodies

1. Vortex briefly (~10 s) a stock solution of 0.54 μm streptavidin-coated polystyrene beads. Dilute 10 μL of beads in 180 μL of Incubation Buffer.
2. Sonicate beads in an ultrasonic bath filled with iced water for several seconds.
3. Add 4 μL of 0.5 mg/mL anti-tubulin antibodies to the bead solution.
4. Incubate at room temperature for 30 min on a rocker.
5. Wash the beads three times by centrifugation at 4500 × *g* for 7 min at 4 °C in 200 μL of Incubation Buffer.
6. Add 4 μL of 40 mM biotinylated PEG to the beads and incubate for 30 min at room temperature on a rocker.
7. Wash the beads three or four times by centrifugation as in **step 5**. After the last centrifugation, resuspend the beads in 100 μL of Incubation Buffer and keep on a rocker at 4 °C for no longer than 3 weeks.

3.5.3 Preparation of Dumbbell Beads Coated with Anti-DIG Antibodies

1. Add 5–10 mg of sulfo-NHS to a clean Eppendorf tube, close the tube and set aside. Add 5–10 mg of EDC to another Eppendorf tube, close the tube and set aside. Write down the exact amounts of reagents in each tube.
2. Briefly vortex (~10 s) a stock solution of carboxylated polystyrene beads. Dilute 4 μL of beads in 96 μL of MES.TWIN Buffer.
3. Sonicate beads for several seconds in an ultrasonic bath filled with iced water.
4. Centrifuge beads at 4500 × *g* for 8 min at 4 °C and resuspend in 120 μL of MES.TWIN Buffer pipetting vigorously.
5. Repeat **steps 3** and **4** until beads are single, as visualized under a microscope.
6. When beads are ready, quickly add ice cold MES.TWIN Buffer to sulfo-NHS and EDC to dissolve these reagents at 50 mg/mL. Immediately, add 40 μL of each solution to 120 μL of bead solution. Pipet well, as the beads will begin to clump.
7. Incubate for 30 min at room temperature on a rocker, vortexing every 5 min to prevent excessive bead clumping.
8. Centrifuge 25 μL of 1 mg/mL anti-DIG Fab fragments at 16,100 × *g* for 5 min at 4 °C. Collect 20 μL of supernatant and keep on ice.
9. Wash the beads three times by adding 200 μL MES.TWIN Buffer and centrifuging as in **step 4**. Pipet vigorously until there are no bead clumps. After the last wash, resuspend in 100 μL of MES.TWIN Buffer.
10. Sonicate beads for several seconds in an ultrasonic bath filled with iced water.
11. Add 20 μL of anti-DIG Fab fragments to the bead solution, mix well by pipetting and incubate overnight on a rocker at 4 °C.
12. Next day, wash beads two times by adding 200 μL MES.TWIN Buffer and centrifuging as in **step 4**. Resuspend in 100 μL of MES.TWIN Buffer.
13. Sonicate beads for several seconds in an ultrasonic bath filled with iced water.
14. To block reactive groups, add 8 μL of 1 M glycine to the bead solution, and incubate for 10 min on a rocker at 4 °C.
15. Wash the beads two times by centrifuging at 4500 × *g* for 8 min at 4 °C in 200 μL of Storage Buffer. After the last centrifugation, resuspend beads in Storage Buffer and keep at 4 °C on a rocker for no longer than 3 weeks (*see* **Note 15**).

3.6 Ultrafast Force-Clamp Assay

In this section, we present the workflow for using the UFFC assay to investigate interactions between various MAPs and MT wall under constant force. This lengthy assay is carried out using two or three microscopy chambers over the course of one experimental day. It involves the following major steps: (1) preparation of chambers with functionalized pedestals; (2) formation of the MT dumbbell; (3) dumbbell stretching; (4) verification of pedestal stability; (5) selection of the z-coordinate to form appropriate contact between the MT dumbbell and functionalized pedestal; and (6) force-clamp measurements. Example results for strong static interactions were generated using the kinesin-7 motor CENP-E in the presence of AMP-PNP, whereas force-induced gliding was demonstrated using the kinetochore-associated Ska protein complex, which exhibits fast diffusion on MT walls (0.1–0.2 $\mu m^2\ s^{-1}$ [21, 71]).

3.6.1 Preparation of a Chamber with Functionalized Pedestals and Stabilized MTs

1. Dumbbell beads are coated with antibodies in advance, as they remain functional for up to 3 weeks (*see* Subheading 3.5). Taxol-stabilized rhodamine-labeled MTs can be used fresh or prepared 1–2 days before the assay. Reagents and protein aliquots are thawed on ice immediately prior to their use in the assays and kept on ice for the duration of experiment (*see* **Note 16**).
2. Turn on all lasers and other equipment and heaters to warm up the instrument.
3. Prepare a flow chamber using a micro-slide, regular coverslip, and double sticky tape spacers. Dilute MT stock 400-fold in 50 μL Assay Buffer and add to the chamber placed on the microscope stage, prewarmed to 32 °C. Use rhodamine or any other appropriate red fluorescence channel to visually inspect the density of MTs floating in the chambers. Adjust the dilution of MT stock to the desired final concentration of MTs (*see* **Note 17**).
4. Prepare a flow chamber with immobilized pedestals (*see* Subheading 3.2) and functionalize with the selected MAP (*see* Subheading 3.4.3). Flow 50 μL MTs of desired concentration.
5. Dilute 4 μL of dumbbell beads fivefold in Assay Buffer prewarmed to room temperature and sonicate for several seconds in an ultrasonic bath filled with iced water. Let the tube with beads to equilibrate to room temperature for 5 min. Carefully add 5 μL of diluted beads to one side of the chamber to avoid extensive mixing of MTs and floating beads (Fig. 9a).
6. Seal both sides of the chamber with Kwik-Cast Sealant.

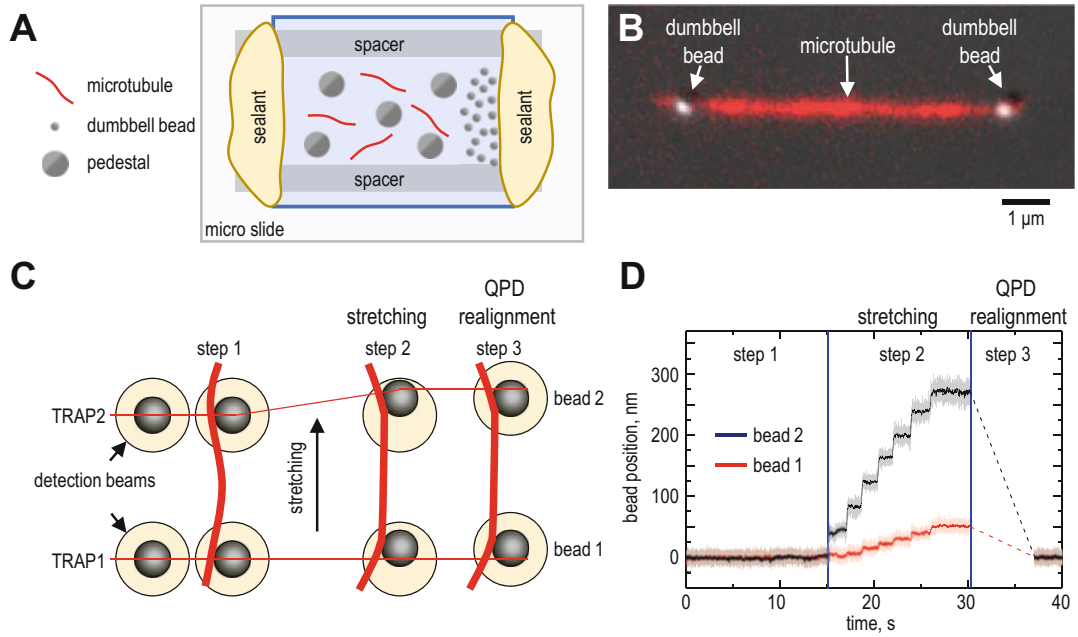

Fig. 9 Dumbbell formation and stretching. (**a**) Schematic of experimental chamber with spatially segregated floating MTs and dumbbell beads. (**b**) An overlay of image of a stretched MT dumbbell (rhodamine channel) and dumbbell beads (DIC). (**c**) Steps to pre-tense MT dumbbell. (**d**) Example signals from two QPDs monitoring dumbbell beads during stretching. Unprocessed signals are shown with light colors, averaged signals are shown with darker lines

3.6.2 Formation of MT Dumbbell

1. Place the chamber prepared using protocol in Subheading 3.6.1 on a prewarmed microscope stage. Make sure to add microscope oil on the condenser, not just the objective side of the chamber, to ensure more even temperature distribution.
2. With the DIC channel, focus inside the chamber 3–5 μm away from the coverslip surface. Using the coarse stage controls, move the stage to the chamber area with floating dumbbell beads. Trap one dumbbell bead in each trapping beam and carefully move the microscope stage back to the area free from floating beads.
3. Visualize captured beads briefly in the rhodamine fluorescence channel to verify the absence of bound MTs. Return to the DIC channel.
4. Carefully adjust the *z*-position of the stage using the piezo-stage control to position trapped beads approximately 2 μm away from the coverslip.
5. Align the tracking and trapping beams (*see* Subheading 3.1.1). Use AOD to move the parental laser beam to carry out criss-cross calibration for both dumbbell beads simultaneously.

6. Carry out stiffness calibration for both traps as described in **step 11** of Subheading 3.1.1. Make sure the stiffnesses of the traps do not differ by more than 20%. For a typical trap stiffness of 0.05 pN/nm, this corresponds to a 0.01 pN/nm difference (*see* **Note 18**).
7. Mark the positions of both beads on the computer screen using any drawing tool such that when switched to the rhodamine channel, the bead locations are apparent.
8. Switch to the rhodamine channel and carefully move the stage to find a floating MT. Select an MT that is 8–12 μm long, 1.2–1.5-fold longer than distance between the trapped dumbbell beads.
9. Using the coarse stage control, put one end of the selected MT in close proximity to one of the trapped beads to encourage binding between the MT end and this bead (*see* **Note 19**).
10. After the contact is established, move the stage to orient the bead-bound MT toward the unattached bead by hydrodynamic drag. Stop moving the stage when the second bead captures MT and the dumbbell appears stable (Fig. 9b) (*see* **Note 20**).

3.6.3 Stretching of MT Dumbbell

During the UFFC assay, the MT dumbbell should be well stretched to establish tension in bead-MT-bead linkages and decrease overall compliance. High pre-tension improves temporal resolution of the assay; however, it also increases probability of dumbbell bead detachment from the MT.

1. Return to the DIC channel and adjust the *z*-position of the stage to place the traps approximately 2 μm from the coverslip.
2. Recalibrate both QPDs using AOD Crisscross Calibration.
3. Begin MT dumbbell stretching procedure by recording the positions of the dumbbell beads. This is schematized as **step 1** in Fig. 9c; the corresponding QPD signals are shown in Fig. 9d.
4. In **step 2**, move one of the traps (TRAP2 in Fig. 9c) at ~1 μm per minute with 50-nm steps. The resultant displacements of two dumbbell beads from the centers of their respective tracking beams will be different, with the bead in the moving TRAP2 exhibiting a greater displacement than the bead in the stationary TRAP1. This difference arises because the pulling force creates a torque on dumbbell beads and bends the dumbbell MT [51].
5. Continue stretching to reach 10 pN pre-tension. Pre-tension force is determined by multiplying the displacement of the bead in the stationary trap by the stiffness of the trap (TRAP1 and bead 1 in Fig. 9c, d).

6. During dumbbell stretching, a bead can occasionally snap back into the trap, releasing the tension without complete detachment from the MT. To avoid this happening during an experiment, the best practice is to stretch the dumbbell up to 10 pN, and then release tension down to 2 pN. Repeat these steps several times to verify that the beads are firmly attached MT wall.
7. Adjust MT dumbbell stretching force to achieve desired pre-tension. We recommend using 2–5 pN pre-tension force because this range provides relatively low noise while maintaining stable dumbbell bead-MT attachment for the duration of a typical UFFC experiment.
8. Repeat AOD crisscross calibration to align the centers of dumbbell beads and corresponding tracking beams (**step 3** in Fig. 9c, d).
9. Start the UFFC program with selected feedback regime (*see* Subheading 3.1.3) to carry out control measurements with a suspended MT dumbbell, which is free from molecular interactions with pedestal. Measurements can be done using up to 350 nm oscillation amplitude (±175 nm; *see* **Note 21**). We routinely start measurements at 4 pN force and examine the range of forces up to 20 pN with 4 pN step (Fig. 10a). With a properly executed force-clamp feedback, dumbbell velocity should be proportional to the clamped force (Fig. 10b, c).

3.6.4 Determining the Contact Point Between MT Dumbbell and MAP-Coated Pedestal

The ultimate goal of this procedure is to bring the stretched MT dumbbell into contact with pedestal so that it can engage in productive and reproducible interactions with the pedestal-bound MAP molecules. If the dumbbell is positioned too far from the pedestal, there will be few MAP binding events, leading to underestimation of the fraction of interacting pedestals. If the dumbbell is pressed too strongly into the pedestal, molecular interactions may be impeded and the signals may become distorted. In the upright microscope, the proper *z*-coordinate for MAP-MT interactions is determined by lowering the stage toward the dumbbell, which is held by two traps ~2 μm away from the coverslip (Fig. 11a). As the coverslip-immobilized pedestal comes in contact with the suspended MT, the MT becomes slightly bent, bringing the dumbbell beads closer to each other. These tiny displacements of the dumbbell beads are monitored by the corresponding QPDs to accurately identify the *z*-coordinate for the onset of inward bead motion. This position corresponds to the pedestal surface and is used for subsequent UFFC measurements.

1. Adjust laser beam that detects position of pedestal bead to bring it in between the trapped dumbbell beads. In our system, *tracking beam 5* is steered using actuator-controlled *mirror 5*

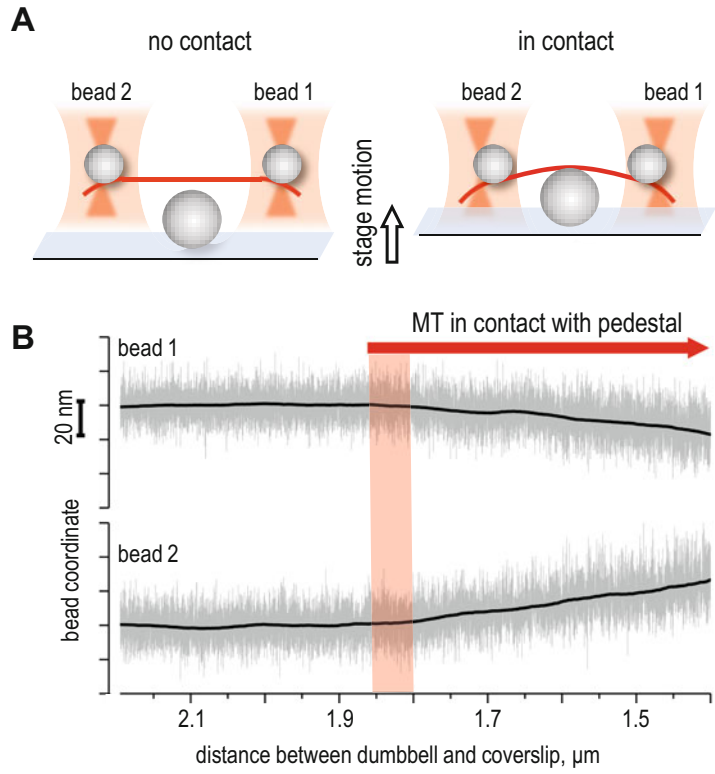

Fig. 10 Typical results for control (free) MT dumbbell. (**a**) Changes in the coordinate of one of the dumbbell beads, and (**b**) corresponding velocity distributions for the indicated force clamped via the Leading Trap Feedback regime. "Up" and "down" directions correspond to the rising and descending segments of bead trajectories shown in (**a**) [53]. (**c**) Velocity of dumbbell motion as a function of force. Each dot represents average velocity for 12–16 experiments, each recording the oscillations of a free MT dumbbell for 30 s. Error bars show SD, data collected from eight chambers. Line is a linear fit constrained at the origin

(Fig. 2b). Zero the *x*- and *y*-axis signals of QPD which monitors the signal from this tracking beam (*QPD3*). Mark beam position on the imaging window on PC monitor using any drawing tool.

2. Using the coarse stage controls, carefully move the stage to find a pedestal that is located away from other pedestals so that they do not interfere with measurements.
3. Bring the selected pedestal close to the middle of the stretched dumbbell MT. Adjust the pedestal position in the *x*-*y* plane, such that its center matches the tracking beam position on the imaging window marked during **step 1**. Use piezo-stage to zero the *x*- and *y*-signals of *QPD3*.

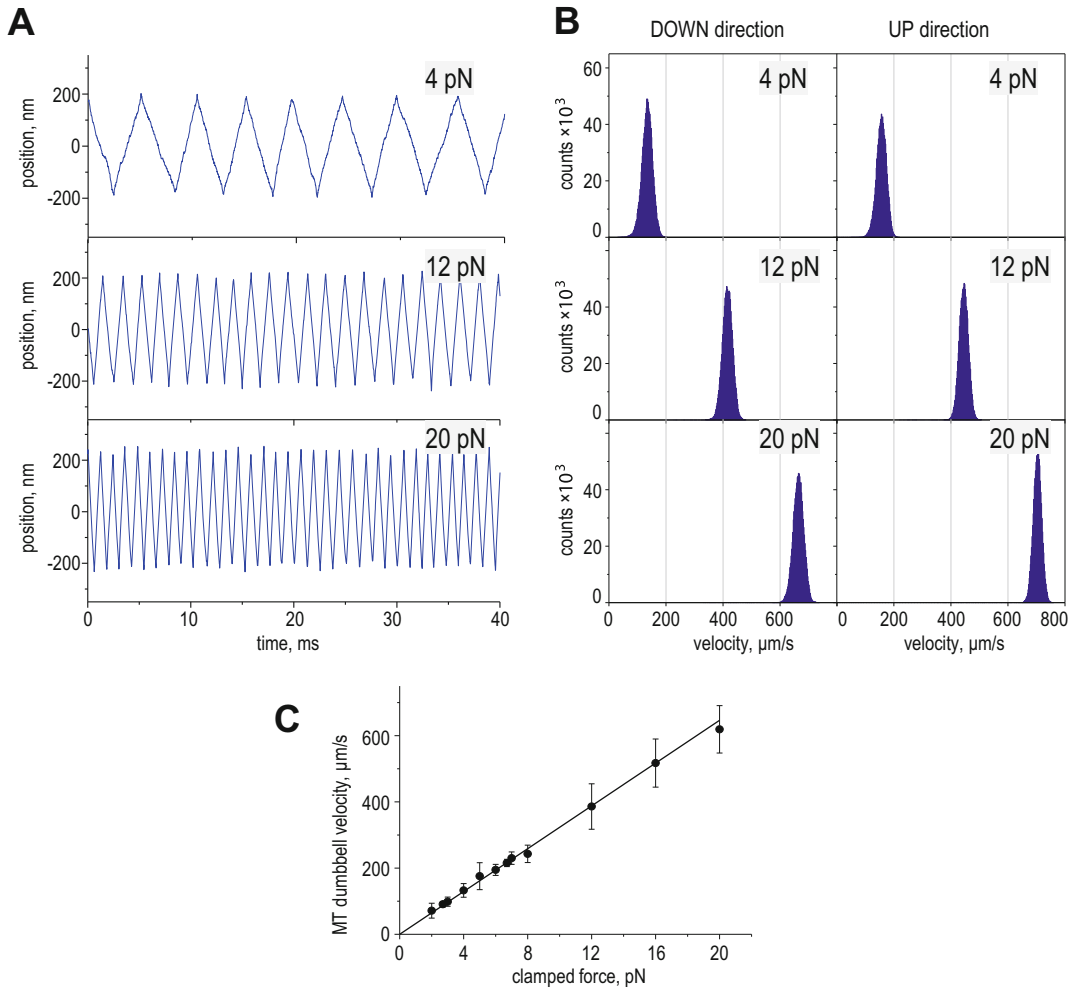

Fig. 11 Determining proper *z*-position for MT dumbbell during UFFC assay. (**a**) Rationale for the procedure to find the surface of pedestal bead. (**b**) Typical recordings of the *y*-coordinates of two dumbbell beads during motion of the piezo-stage, which brings the dumbbell closer to the coverslip with immobilized 1.8 μm pedestal. Diffuse red bar marks the approximate location of the pedestal surface

4. Slowly move the piezo-stage up to 1 μm toward the MT dumbbell at 10 μm per minute while monitoring the *y*-axis QPD signals for both dumbbell beads (Fig. 11b). Find the approximate coordinate at which the dumbbell beads start moving toward each other and select this *z*-position as the MT-pedestal contact point for the UFFC assay.

3.6.5 Verification of Pedestal Stability

To ensure accurate measurements, the stability of each pedestal should be tested prior to the UFFC assay. If the pedestal is deemed sufficiently stable, the feedback control for stage stabilization is engaged (*see* Subheading 3.1.2). If the pedestal is shaky, it is

abandoned, and the steps described in Subheading 3.6.4 are repeated for a new pedestal.

1. To avoid touching the pedestal surface with an MT dumbbell during this procedure, move the piezo-stage along the *z*-axis 200 nm away from the contact point. Then, use AOD to move the MT dumbbell along the *x*-axis, which is perpendicular to the MT axis, to separate the MT dumbbell and pedestal by ~2 μm.
2. Perform stage crisscross calibration and save these data to a file, which will be used for real-time stage stabilization program.
3. Move the MT dumbbell along *x*-axis to return it to pedestal. Check the *y*-axis voltage signals on two QPDs monitoring the dumbbell beads (*QPDs 1* and *2*). If these readings are zero, the MT dumbbell remains under tension. If the *y*-axis signals exceed 5 nm and the change on *QPD1* and *QPD2* is in opposite directions, the MT dumbbell tension has decreased. In this case, release pre-tension completely by using actuator-driven gimbal *mirror 2* (Fig. 2b) to move TRAP2 toward TRAP1 until the *y*-axis QPD signal for dumbbell bead 1 stops responding. Stretch the MT dumbbell again by following instructions in Subheading 3.6.3 starting from **step 2**.
4. With *QPD3*, record the *x,y* position of the pedestal for 5 s and calculate the SD with a 100-ms sliding window (*see* Subheading 3.3.1). If the SD for pedestal's thermal vibrations is less than 5 nm, engage the stage stabilization program and proceed to the UFFC assay. Otherwise, find another pedestal and repeat, starting from Subheading 3.6.4.

3.6.6 Ultrafast Force-Clamp Measurements

1. Immediately after accomplishing the steps described in Subheadings 3.6.4 and 3.6.5, start the UFFC program (*see* Subheading 3.1.3). We routinely implement "Leading Trap Feedback" at 4 pN force, oscillating the dumbbell for 30 s. For each measurement, the program saves the *y*-coordinates of both dumbbell beads recorded by *QPDs 1* and *2*, as well as the *y*-coordinates of both traps.
2. After the measurements stop, visually scan the signal from one of the dumbbell QPDs. If oscillations proceed in a regular pattern and bead trajectory looks the same as in the control signal collected some distance away from the pedestal (Fig. 10), proceed to the next pedestal and repeat the procedures, starting from Subheading 3.6.4.
3. If the dumbbell signal contains pauses (Fig. 12a) or segments with reduced dumbbell velocity (Fig. 13a), the MT likely interacted with the pedestal-immobilized MAP molecule(s). In this case, measurements should be continued at other force values, to collect data for the force-sensitivity of these interactions.

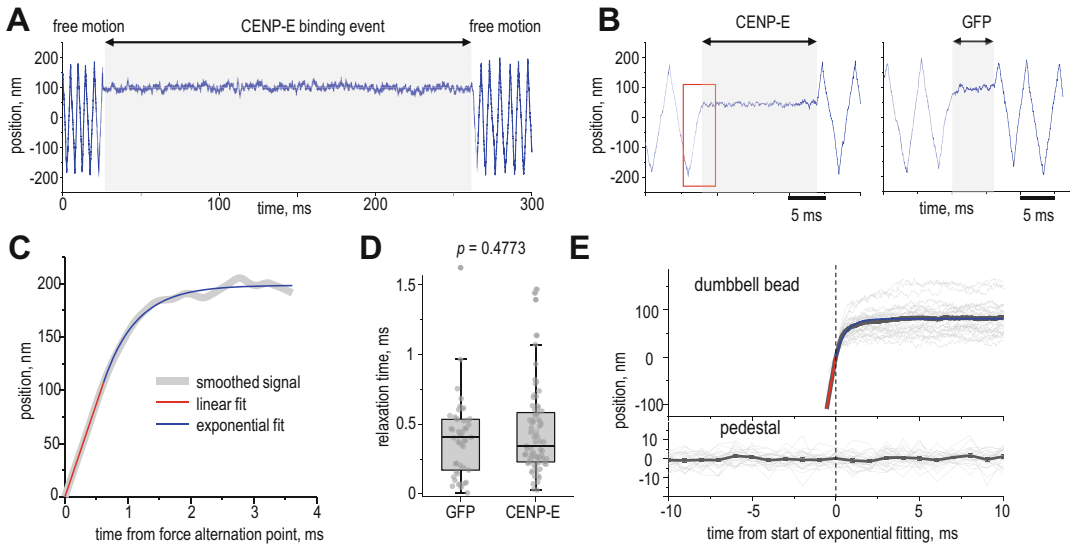

Fig. 12 Static MT-binding interactions. (**a**) Example UFFC recording showing changes in the position of one of the dumbbell beads near the pedestal coated with GFP-tagged CENP-E kinesin in the buffer with 1 mM AMP-PNP. Gray area highlights one binding event, during which the dumbbell maintains its position under 4 pN force. (**b**) Example recordings with a brief CENP-E binding event and a typical GFP-binding event. (**c**) Enlarged onset of the binding event shown by the red box in panel B. Time zero corresponds to the change in force direction, which led to the upward segment of bead trajectory immediately prior to the binding event. A trajectory smoothed using local regression (LOESS; 2.5 ms window) was fitted with a combination of a linear function and a single-exponential function with minimal R^2; signals in which the amplitude of one of the functions was $<10\%$ were discarded. The characteristic time for single-exponential fit describes dumbbell stopping upon molecular binding with strong affinity. (**d**) Characteristic times for the onset of binding events observed with CENP-E ($n = 77$) and GFP ($n = 49$) at 4 pN. Bars shown with median lines and 1.5 inter quartile ranges, p-value determined by Mann–Whitney test. (**e**) Top graph shows individual curves (gray) for the onset of binding events for CENP-E in the presence of AMP-PNP. These curves were aligned to match the start of exponential fittings. The average signal was fitted using linear (red) and exponential (blue) functions. The same binding events were examined to plot changes in the y-position of the pedestal bead along the force application axis (bottom graph). The absence of a shift in pedestal position upon CENP-E binding confirms the high stability of pedestal immobilization

Input the desired clamp force value and repeat the measurement, starting from **step 1** and without introducing any changes to the dumbbell, trapping or tracking beams. We usually collect data for four or five different force values for each interacting pedestal.

4. Proceed to the next pedestal and repeat the procedures starting from Subheading 3.6.4. We routinely work with one chamber for 1–2 h, collecting data for 10–14 pedestals with the help of 1–3 MT dumbbells.
5. After finishing UFFC measurements, turn off the lasers, switch to the GFP fluorescence imaging channel, and record z-stacks over 1.5 μm with 200-nm steps of at least 30 pedestals for

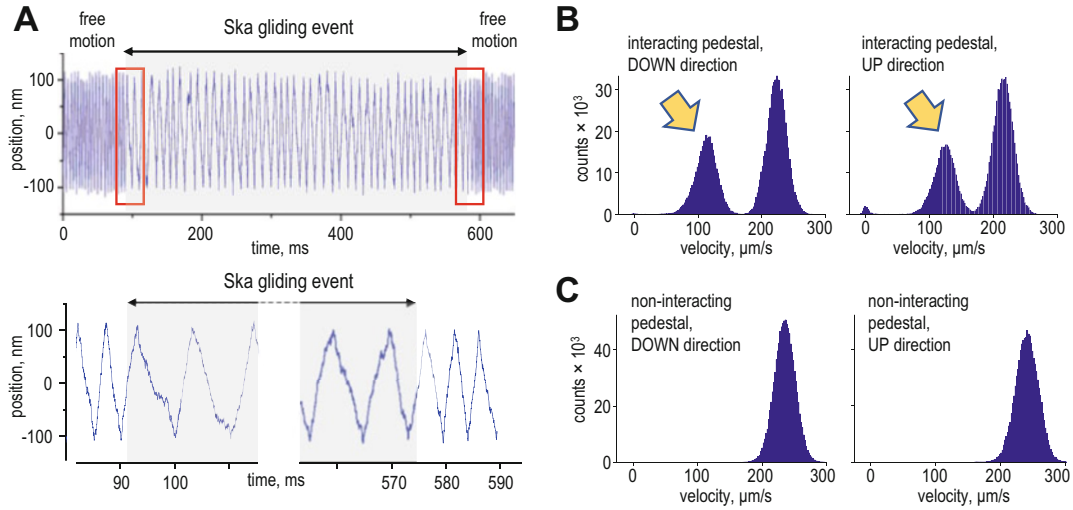

Fig. 13 Friction-generating gliding of the full-length Ska complex along MT under force. (**a**) Example signal with a processive gliding event (gray box) recorded at 6 pN. Close-up views of segments at the start and end of gliding (red boxes) are shown below. (**b**, **c**) Velocity distributions for MT dumbbell motion plotted for different directions for Ska-coated pedestals that showed interactions (**b**) or not (**c**). Gliding events lead to appearance of peaks with low velocity (arrows). Position of free velocity peaks is slightly different owing to experimental variables, such as different MT dumbbells, experimental chambers and optical alignments

subsequent analysis of GFP fluorescence brightness (*see* Subheading 3.4).

3.6.7 Data Analysis

A typical UFFC experiment acquires vast volumes of data for MAP–MT interactions, as coordinates for both dumbbell beads are collected at 66 kHz for 30 s at each force value. Analyzing these interactions is far from trivial, and will require specialized algorithms. Below, we provide a brief description of recommended controls and expected results.

1. *Quality controls.* Initial analysis of recorded data should include visual inspection of all signals to identify recordings that show clear deviations, e.g., those in which the difference in free velocities of two dumbbell beads exceeds 30%. Control recordings obtained with free MT dumbbells (suspended away from pedestals) or with MT dumbbells oscillated near the GFP-coated pedestals, as well as experimental signals collected with the MAP-coated pedestals that showed no interactions, should exhibit symmetric triangular trajectories (Fig. 10a). The distributions of instantaneous velocities for each direction of motion, prepared as in [53], should be highly similar in amplitude and width (Fig. 10b), and should show an average velocity that increases linearly with input force (Fig. 10c). Another important quality control is examination of the length of the MT dumbbell during oscillations, which can be obtained by

subtracting the positions of the dumbbell beads along the MT axis. Small changes in MT dumbbell length are often observed upon MT–MAP binding at large forces (>16 pN), and they appear to be unavoidable with current procedures for dumbbell preparation. However, we discard all signals that exhibit an abrupt increase in the bead-to-bead distance over 10 nm, which indicates the loss of the desired pre-tension of the MT dumbbell.

2. *Static interactions.* Non-processive binding events are observed between the MT and proteins with high MT-binding affinity, as illustrated in Fig. 12a using the Kinesin-7 motor CENP-E in the presence of AMP-PNP, a non-hydrolysable analogue of ATP. Distribution of the durations of MAP-MT bindings as a function of force provides invaluable information about the underlying interaction mechanisms. Such analyses can be carried out as described for other protein–filament interactions [41, 42, 55]. Another important characteristic of static binding is the kinetics of the transition from free MT dumbbell motion to a binding-induced stall. Before CENP-E kinesin molecule contacts the MT, the dumbbell travels at a constant (free) velocity corresponding to the clamped force, and upon CENP-E binding the motion gradually slows down before coming to a stop. Similar pauses, albeit much rarer and with shorter durations, can be detected between the MT dumbbell and control pedestals coated with GFP, representing nonspecific binding events (Fig. 12b). The exponential transitions from the free velocity segment to the plateau at stall have similar characteristic times for kinesin CENP-E and GFP (~0.4 ms) (Fig. 12c, d), implying that the kinetics of this transition is a property of the dumbbell, not the MT-bound proteins. Interestingly, this relaxation time is noticeably longer than reported previously for actin-containing dumbbells [44], although the direct comparison is difficult due to different experimental conditions. To verify that the kinetics of such transitions are not affected by pedestal tilting, changes in pedestal position should be analyzed during the onset of binding events (Fig. 12e).
3. *Gliding MAPs.* When a diffusive MAP immobilized onto the pedestal contacts a moving MT, it can exhibit a gliding motion, resulting in a reduction of the dumbbell velocity. In general, friction generation in the gliding state, and therefore the velocity of gliding, are defined by the binding energy between the MAP molecule and its MT-binding site [15–17]. Such processive interactions are visible in UFFC recordings of the dumbbell bead coordinate vs. time as segments with slower than normal dumbbell velocity (Fig. 13a). Distributions of instantaneous velocities plotted for each direction of motion reveal

distinct peaks with low velocities, as well as peaks that correspond to free motion seen with the control dumbbell (Fig. 13b). For the kinetochore-associated Ska complex, gliding velocity is similar in both MT directions, consistent with prior finding that the MT-binding domain of the Ska complex is not stereospecific [72]. Some MAPs are expected to exhibit slightly asymmetric velocities in this assay [17, 19], although this prediction has not yet been tested, and a mechanistic theory to explain different MAP gliding behaviors has not yet been developed. UFFC spectroscopy provides a powerful tool for examining the gliding properties of various MAPs and elucidating the mechanism of MAPs' ability to translocate processively along MT wall under variable force.

4 Notes

1. To implement the UFFC, an AOD can be replaced with an electro-optical deflector, which exhibits more uniform modulation of the trapping beam and a faster response time [54]. Nonuniform modulation, however, is of lesser significance in laser-tweezers systems with dedicated tracking beams that are not steered by AOD.
2. In this optical scheme, the two tracking beams for the dumbbell beads have different wavelengths. It is also possible to monitor both dumbbell beads using a single laser beam which is split into two beams based on polarization (e.g., *tracking beams 1* and *2*, or *tracking beams 3* and *4*, Fig. 2b). This detection scheme, however, is incompatible with DIC optics, which alters light polarization and leads to a significant crosstalk.
3. Bead immobilization via partial melting should be done with regular coverslips because bead solution does not spread well on hydrophobic surface of a silanized coverslip.
4. Heating for >30 s at 100 °C causes polystyrene beads to start losing their shape.
5. Moist paper towel prevents chamber from drying for many hours. However, avoid water condensation on the sticky tape surface, which may lead to tape's detachment.
6. We silanize coverslips as in [73], except the initial cleaning is done with a plasma cleaner for 15 min at 30 W.
7. The pedestal stability test via laser trap oscillation is helpful during troubleshooting a pedestal immobilization protocol. For routine experiments, the SD method is more appropriate because it is easier and faster to implement.

8. Procedures for quantifying the brightness of GFP beads, as well as other tips for preparing protein-coated beads, can be found in [68].
9. Partially melted beads do not functionalize well using this method, but they can be coated using biotinylated anti-GFP antibodies.
10. To minimize nonspecific interactions between MAPs and streptavidin, the surface of the pedestals can also be blocked with biotinylated BSA.
11. There are many different computer programs to quantify bead brightness, e.g., the Time-Series Analyzer plugin for the ImageJ software https://imagej.nih.gov/ij/plugins/time-series.html.
12. Partially melted pedestals consistently provide fewer interacting events than the pedestals immobilized via nonspecific adsorption even when the partially melted pedestals are functionalized using a relatively high concentration of Ndc80-GFP (Fig. 8). High temperature appears to increase stickiness of pedestal beads, leading to inactivation of nonspecifically adsorbed Ndc80-GFP. Thus, although partially melted pedestals have high mechanical stability, this immobilization approach may not work for some proteins.
13. Because degree of tubulin labeling varies from experiment to experiment, the optimal ratio of tubulins in this mix should be determined empirically for each tubulin preparation. In general, the fraction of modified tubulins should be kept to the minimum sufficient for strong bead attachment (DIG) and MT visualization (rhodamine).
14. If DIG-labeled tubulin is added to the tubulin mixture, incubation time should be increased up to 30 min.
15. Beads coated with anti-DIG antibodies can also be prepared using streptavidin-coated beads. In this case, follow the protocol in Subheading 3.5.2 using biotinylated primary antibodies and anti-DIG antibodies. This protocol is faster, but dumbbell beads prepared with streptavidin-coated polystyrene beads tend to aggregate more strongly than carboxylated beads.
16. For other tips on handling proteins for in vitro reconstruction experiments, *see* ref. [68].
17. High concentration of soluble MTs may cause binding of multiple MTs to the dumbbell beads during the UFFC assay, whereas at low MT concentration it may be difficult to quickly find an MT to form a dumbbell. Hence, we suggest optimizing MT concentration before adding the MTs into experimental flow chamber with immobilized pedestal beads.

18. Unequal stiffness can be caused by unequal bead size, the presence of an additional MT attached to one of the beads, unequal laser intensity in dual traps or other factors.
19. While searching for an MT, avoid moving the trapped beads deeper than ~7 μm from the coverslip, as the beads may escape due to decreased trap stiffness.
20. The manipulation time should be minimized to avoid bleaching and destroying the MTs.
21. The dumbbell oscillation amplitude is limited by the QPD's response range.

Acknowledgments

We gratefully thank Drs. Yale E. Goldman and Michael Ostap, and their lab members, for their continuous support and excellent suggestions over the years as we developed the protocols and methods detailed herein. We also thank members of our lab for stimulating discussions and technical assistance. This work is supported by the National Institute of General Medical Sciences of the National Institutes of Health under award numbers R35-GM141747 to E.L.G, and the National Science Foundation (grant #2029868). Development of protocols to functionalize pedestals and microscopy chambers was supported in part by a grant from the Russian Science Foundation (project No. 21-45-00012).

References

1. Peterman EJ, Scholey JM (2009) Mitotic microtubule crosslinkers: insights from mechanistic studies. Curr Biol 19(23): R1089–R1094. https://doi.org/10.1016/j.cub.2009.10.047
2. Akhmanova A, Steinmetz MO (2015) Control of microtubule organization and dynamics: two ends in the limelight. Nat Rev Mol Cell Biol 16(12):711–726. https://doi.org/10.1038/nrm4084
3. Bodakuntla S, Jijumon AS, Villablanca C, Gonzalez-Billault C, Janke C (2019) Microtubule-associated proteins: structuring the cytoskeleton. Trends Cell Biol 29(10): 804–819. https://doi.org/10.1016/j.tcb.2019.07.004
4. Tripathy SK, Weil SJ, Chen C, Anand P, Vallee RB, Gross SP (2014) Autoregulatory mechanism for dynactin control of processive and diffusive dynein transport. Nat Cell Biol 16(12):1192–U1147. https://doi.org/10.1038/ncb3063
5. Barlan K, Gelfand VI (2017) Microtubule-based transport and the distribution, tethering, and organization of organelles. Cold Spring Harb Perspect Biol 9(5):a025817. https://doi.org/10.1101/cshperspect.a025817
6. van de Willige D, Hoogenraad CC, Akhmanova A (2016) Microtubule plus-end tracking proteins in neuronal development. Cell Mol Life Sci 73(10):2053–2077. https://doi.org/10.1007/s00018-016-2168-3
7. Ramkumar A, Jong BY, Ori-McKenney KM (2018) ReMAPping the microtubule landscape: how phosphorylation dictates the activities of microtubule-associated proteins. Dev Dyn 247(1):138–155. https://doi.org/10.1002/dvdy.24599
8. Sferra A (2020) Microtubule dysfunction: a common feature of neurodegenerative

diseases. Int J Mol Sci 21(19):7354. https://doi.org/10.3390/ijms21197354

9. Cheeseman IM (2014) The kinetochore. Cold Spring Harb Perspect Biol 6(7):a015826. https://doi.org/10.1101/cshperspect.a015826
10. Musacchio A, Desai A (2017) A molecular view of kinetochore assembly and function. Biology (Basel) 6(1):5. https://doi.org/10.3390/biology6010005
11. Grishchuk EL (2017) Biophysics of microtubule end coupling at the kinetochore. Prog Mol Subcell Biol 56:397–428. https://doi.org/10.1007/978-3-319-58592-5_17
12. Joglekar AP, Bloom KS, Salmon ED (2010) Mechanisms of force generation by end-on kinetochore-microtubule attachments. Curr Opin Cell Biol 22(1):57–67. https://doi.org/10.1016/j.ceb.2009.12.010
13. Maddox P, Straight A, Coughlin P, Mitchison TJ, Salmon ED (2003) Direct observation of microtubule dynamics at kinetochores in Xenopus extract spindles: implications for spindle mechanics. J Cell Biol 162(3):377–382. https://doi.org/10.1083/jcb.200301088
14. Dumont S, Salmon ED, Mitchison TJ (2012) Deformations within moving kinetochores reveal different sites of active and passive force generation. Science 337(6092):355–358. https://doi.org/10.1126/science.1221886
15. Efremov A, Grishchuk EL, McIntosh JR, Ataullakhanov FI (2007) In search of an optimal ring to couple microtubule depolymerization to processive chromosome motions. Proc Natl Acad Sci U S A 104(48):19017–19022. https://doi.org/10.1073/pnas.0709524104
16. Hill TL (1985) Theoretical problems related to the attachment of microtubules to kinetochores. Proc Natl Acad Sci 82(13):4404–4408. https://doi.org/10.1073/pnas.82.13.4404
17. Bormuth V, Varga V, Howard J, Schaffer E (2009) Protein friction limits diffusive and directed movements of kinesin motors on microtubules. Science 325(5942):870–873. https://doi.org/10.1126/science.1174923
18. Grishchuk EL, Spiridonov IS, Volkov VA, Efremov A, Westermann S, Drubin D, Barnes G, Ataullakhanov FI, McIntosh JR (2008) Different assemblies of the DAM1 complex follow shortening microtubules by distinct mechanisms. Proc Natl Acad Sci U S A 105(19):6918–6923. https://doi.org/10.1073/pnas.0801811105
19. Forth S, Hsia KC, Shimamoto Y, Kapoor TM (2014) Asymmetric friction of nonmotor MAPs can lead to their directional motion in active microtubule networks. Cell 157(2):420–432. https://doi.org/10.1016/j.cell.2014.02.018
20. Lansky Z, Braun M, Ludecke A, Schlierf M, ten Wolde PR, Janson ME, Diez S (2015) Diffusible crosslinkers generate directed forces in microtubule networks. Cell 160(6):1159–1168. https://doi.org/10.1016/j.cell.2015.01.051
21. Chakraborty M, Tarasovetc EV, Zaytsev AV, Godzi M, Figueiredo AC, Ataullakhanov FI, Grishchuk EL (2019) Microtubule end conversion mediated by motors and diffusing proteins with no intrinsic microtubule end-binding activity. Nat Commun 10(1):1673. https://doi.org/10.1038/s41467-019-09411-7
22. Gaska I, Armstrong ME, Alfieri A, Forth S (2020) The mitotic crosslinking protein PRC1 acts like a mechanical dashpot to resist microtubule sliding. Dev Cell 54(3):367. https://doi.org/10.1016/j.devcel.2020.06.017
23. Okada Y, Hirokawa N (2000) Mechanism of the single-headed processivity: diffusional anchoring between the K-loop of kinesin and the C terminus of tubulin. Proc Natl Acad Sci U S A 97(2):640–645. https://doi.org/10.1073/pnas.97.2.640
24. Cooper JR, Wordeman L (2009) The diffusive interaction of microtubule binding proteins. Curr Opin Cell Biol 21(1):68–73. https://doi.org/10.1016/j.ceb.2009.01.005
25. Zaytsev AV, Mick JE, Maslennikov E, Nikashin B, DeLuca JG, Grishchuk EL (2015) Multisite phosphorylation of the NDC80 complex gradually tunes its microtubule-binding affinity. Mol Biol Cell 26(10):1829–1844. https://doi.org/10.1091/mbc.E14-11-1539
26. Brouhard GJ, Stear JH, Noetzel TL, Al-Bassam J, Kinoshita K, Harrison SC, Howard J, Hyman AA (2008) XMAP215 is a processive microtubule polymerase. Cell 132(1):79–88. https://doi.org/10.1016/j.cell.2007.11.043
27. Hinrichs MH, Jalal A, Brenner B, Mandelkow E, Kumar S, Scholz T (2012) Tau protein diffuses along the microtubule lattice. J Biol Chem 287(46):38559–38568. https://doi.org/10.1074/jbc.M112.369785
28. Ashkin A, Dziedzic JM, Bjorkholm JE, Chu S (1986) Observation of a single-beam gradient force optical trap for dielectric particles. Opt Lett 11(5):288–290. https://doi.org/10.1364/ol.11.000288
29. Finer JT, Simmons RM, Spudich JA (1994) Single myosin molecule mechanics:

piconewton forces and nanometre steps. Nature 368(6467):113–119. https://doi.org/10.1038/368113a0

30. Visscher K, Schnitzer MJ, Block SM (1999) Single kinesin molecules studied with a molecular force clamp. Nature 400(6740):184–189. https://doi.org/10.1038/22146
31. Capitanio M, Pavone FS (2013) Interrogating biology with force: single molecule high-resolution measurements with optical tweezers. Biophys J 105(6):1293–1303. https://doi.org/10.1016/j.bpj.2013.08.007
32. Pyrpassopoulos S, Shuman H, Ostap EM (2020) Modulation of Kinesin's load-bearing capacity by force geometry and the microtubule track. Biophys J 118(1):243–253. https://doi.org/10.1016/j.bpj.2019.10.045
33. Schnitzer MJ, Visscher K, Block SM (2000) Force production by single kinesin motors. Nat Cell Biol 2(10):718–723. https://doi.org/10.1038/35036345
34. Gennerich A, Carter AP, Reck-Peterson SL, Vale RD (2007) Force-induced bidirectional stepping of cytoplasmic dynein. Cell 131(5):952–965. https://doi.org/10.1016/j.cell.2007.10.016
35. Laakso JM, Lewis JH, Shuman H, Ostap EM (2008) Myosin I can act as a molecular force sensor. Science 321(5885):133–136. https://doi.org/10.1126/science.1159419
36. Andreasson Johan OL, Shastry S, Hancock William O, Block Steven M (2015) The mechanochemical cycle of mammalian kinesin-2 KIF3A/B under load. Curr Biol 25(9):1166–1175. https://doi.org/10.1016/j.cub.2015.03.013
37. Gudimchuk N, Tarasovetc EV, Mustyatsa V, Drobyshev AL, Vitre B, Cleveland DW, Ataullakhanov FI, Grishchuk EL (2018) Probing mitotic CENP-E kinesin with the tethered cargo motion assay and laser tweezers. Biophys J 114(11):2640–2652. https://doi.org/10.1016/j.bpj.2018.04.017
38. Uemura S, Si I (2003) Loading direction regulates the affinity of ADP for kinesin. Nat Struct Mol Biol 10(4):308–311. https://doi.org/10.1038/nsb911
39. Oguchi Y, Mikhailenko SV, Ohki T, Olivares AO, De La Cruz EM, Si I (2008) Load-dependent ADP binding to myosins V and VI: implications for subunit coordination and function. Proc Natl Acad Sci 105(22):7714–7719. https://doi.org/10.1073/pnas.0800564105
40. Cleary FB, Dewitt MA, Bilyard T, Htet ZM, Belyy V, Chan DD, Chang AY, Yildiz A (2014) Tension on the linker gates the ATP-dependent release of dynein from microtubules. Nat Commun 5:4587. https://doi.org/10.1038/ncomms5587
41. Dogan Merve Y, Can S, Cleary Frank B, Purde V, Yildiz A (2015) Kinesin's front head is gated by the backward orientation of its neck linker. Cell Rep 10(12):1967–1973. https://doi.org/10.1016/j.celrep.2015.02.061
42. Buckley CD, Tan J, Anderson KL, Hanein D, Volkmann N, Weis WI, Nelson WJ, Dunn AR (2014) Cell adhesion. The minimal cadherin-catenin complex binds to actin filaments under force. Science 346(6209):1254211. https://doi.org/10.1126/science.1254211
43. Huang DL, Bax NA, Buckley CD, Weis WI, Dunn AR (2017) Vinculin forms a directionally asymmetric catch bond with F-actin. Science 357(6352):703–706. https://doi.org/10.1126/science.aan2556
44. Capitanio M, Canepari M, Maffei M, Beneventi D, Monico C, Vanzi F, Bottinelli R, Pavone FS (2012) Ultrafast force-clamp spectroscopy of single molecules reveals load dependence of myosin working stroke. Nat Methods 9(10):1013–1019. https://doi.org/10.1038/nmeth.2152
45. Svoboda K, Block SM (1994) Force and velocity measured for single kinesin molecules. Cell 77(5):773–784. pii:0092-8674(94)90060-4
46. Grishchuk EL, Molodtsov MI, Ataullakhanov FI, McIntosh JR (2005) Force production by disassembling microtubules. Nature 438(7066):384–388. https://doi.org/10.1038/nature04132
47. Grishchuk EL, Efremov AK, Volkov VA, Spiridonov IS, Gudimchuk N, Westermann S, Drubin D, Barnes G, McIntosh JR, Ataullakhanov FI (2008) The Dam1 ring binds microtubules strongly enough to be a processive as well as energy-efficient coupler for chromosome motion. Proc Natl Acad Sci U S A 105(40):15423–15428. https://doi.org/10.1073/pnas.0807859105
48. Sung J, Nag S, Mortensen KI, Vestergaard CL, Sutton S, Ruppel K, Flyvbjerg H, Spudich JA (2015) Harmonic force spectroscopy measures load-dependent kinetics of individual human beta-cardiac myosin molecules. Nat Commun 6:7931. https://doi.org/10.1038/ncomms8931
49. Howard J, Hancock WO (2020) Three beads are better than one. Biophys J 118(1):1–3. https://doi.org/10.1016/j.bpj.2019.12.001
50. Gardini L, Woody MS, Kashchuk AV, Goldman YE, Ostap EM, Capitanio M (2022) High-speed optical traps address dynamics of processive and non-processive molecular motors. In:

Gennerich A (ed) Optical tweezers: methods and protocols. Methods in molecular biology, vol 2478. Springer, New York

51. Dupuis DE, Guilford WH, Wu J, Warshaw DM (1997) Actin filament mechanics in the laser trap. J Muscle Res Cell Motil 18(1):17–30. https://doi.org/10.1023/a:1018672631256
52. Arbore C, Sergides M, Gardini L, Pavone FS, Capitanio M (2020) α-Catenin switches between a slip and a cooperative catch bond with F-actin to regulate cell junction fluidity. bioRxiv:2020.2004.2015.035527. https://doi.org/10.1101/2020.04.15.035527
53. Gardini L, Tempestini A, Pavone FS, Capitanio M (2018) High-speed optical tweezers for the study of single molecular motors. Methods Mol Biol 1805:151–184. https://doi.org/10.1007/978-1-4939-8556-2_9
54. Woody MS, Capitanio M, Ostap EM, Goldman YE (2018) Electro-optic deflectors deliver advantages over acousto-optical deflectors in a high resolution, ultra-fast force-clamp optical trap. Opt Express 26(9):11181–11193. https://doi.org/10.1364/OE.26.011181
55. Woody MS, Winkelmann DA, Capitanio M, Ostap EM, Goldman YE (2019) Single molecule mechanics resolves the earliest events in force generation by cardiac myosin. elife 8. https://doi.org/10.7554/eLife.49266
56. Tempestini A, Monico C, Gardini L, Vanzi F, Pavone FS, Capitanio M (2018) Sliding of a single lac repressor protein along DNA is tuned by DNA sequence and molecular switching. Nucleic Acids Res 46(10):5001–5011. https://doi.org/10.1093/nar/gky208
57. Howard J (2001) Mechanics of motor proteins and the cytoskeleton. Sinauer Associates, Sunderland
58. Brouhard GJ, Schek HT 3rd, Hunt AJ (2003) Advanced optical tweezers for the study of cellular and molecular biomechanics. IEEE Trans Biomed Eng 50(1):121–125. https://doi.org/10.1109/TBME.2002.805463
59. Barisic M, Silva e Sousa R, Tripathy SK, Magiera MM, Zaytsev AV, Pereira AL, Janke C, Grishchuk EL, Maiato H (2015) Mitosis. Microtubule detyrosination guides chromosomes during mitosis. Science 348(6236):799–803. https://doi.org/10.1126/science.aaa5175
60. Sung JM, Sivaramakrishnan S, Dunn AR, Spudich JA (2010) Single-molecule dual-beam optical trap analysis of protein structure and function. Method Enzymol 475:321–375. https://doi.org/10.1016/S0076-6879(10)75014-X
61. Visscher K, Block SM (1998) Versatile optical traps with feedback control. Methods Enzymol 298:460–489. https://doi.org/10.1016/s0076-6879(98)98040-5
62. Greenberg MJ, Shuman H, Ostap EM (2017) Measuring the kinetic and mechanical properties of non-processive Myosins using optical tweezers. In: Gennerich A (ed) Optical tweezers: methods and protocols. Springer, New York, pp 483–509. https://doi.org/10.1007/978-1-4939-6421-5_19
63. Cheeseman IM, Desai A (2008) Molecular architecture of the kinetochore-microtubule interface. Nat Rev Mol Cell Biol 9(1):33–46. https://doi.org/10.1038/nrm2310
64. Pristoupil TI, Kramlova M, Sterbikova J (1969) On the mechanism of adsorption of proteins to nitrocellulose in membrane chromatography. J Chromatogr 42(3):367–375. https://doi.org/10.1016/s0021-9673(01)80636-1
65. Ciferri C, Pasqualato S, Screpanti E, Varetti G, Santaguida S, Dos Reis G, Maiolica A, Polka J, De Luca JG, De Wulf P, Salek M, Rappsilber J, Moores CA, Salmon ED, Musacchio A (2008) Implications for kinetochore-microtubule attachment from the structure of an engineered Ndc80 complex. Cell 133(3):427–439. https://doi.org/10.1016/j.cell.2008.03.020
66. Waner MJ, Navrotskaya I, Bain A, Oldham ED, Mascotti DP (2004) Thermal and sodium dodecylsulfate induced transitions of streptavidin. Biophys J 87(4):2701–2713. https://doi.org/10.1529/biophysj.104.047266
67. Li Q, King Stephen J, Gopinathan A, Xu J (2016) Quantitative determination of the probability of multiple-motor transport in bead-based assays. Biophys J 110(12):2720–2728. https://doi.org/10.1016/j.bpj.2016.05.015
68. Chakraborty M, Tarasovetc EV, Grishchuk EL (2018) In vitro reconstitution of lateral to end-on conversion of kinetochore-microtubule attachments. Methods Cell Biol 144:307–327. https://doi.org/10.1016/bs.mcb.2018.03.018
69. Miller HP, Wilson L (2010) Preparation of microtubule protein and purified tubulin from bovine brain by cycles of assembly and disassembly and phosphocellulose chromatography. Methods Cell Biol 95:3–15. https://doi.org/10.1016/S0091-679X(10)95001-2
70. Hyman A, Drechsel D, Kellogg D, Salser S, Sawin K, Steffen P, Wordeman L, Mitchison T (1991) Preparation of modified tubulins. Methods Enzymol 196:478–485. https://doi.org/10.1016/0076-6879(91)96041-o

71. Schmidt JC, Arthanari H, Boeszoermenyi A, Dashkevich NM, Wilson-Kubalek EM, Monnier N, Markus M, Oberer M, Milligan RA, Bathe M, Wagner G, Grishchuk EL, Cheeseman IM (2012) The kinetochore-bound Ska1 complex tracks depolymerizing microtubules and binds to curved protofilaments. Dev Cell 23(5):968–980. https://doi.org/10.1016/j.devcel.2012.09.012
72. Monda JK, Whitney IP, Tarasovetc EV, Wilson-Kubalek E, Milligan RA, Grishchuk EL, Cheeseman IM (2017) Microtubule tip tracking by the spindle and kinetochore protein Ska1 requires diverse tubulin-interacting surfaces. Curr Biol 27(23):3666–3675.e3666. https://doi.org/10.1016/j.cub.2017.10.018
73. Volkov VA, Zaytsev AV, Grishchuk EL (2014) Preparation of segmented microtubules to study motions driven by the disassembling microtubule ends. J Vis Exp (85):51150. https://doi.org/10.3791/51150